Targeting 5-HT 2B Receptor Signaling Prevents Border Zone Expansion and Improves Microstructural Remodeling after Myocardial Infarction

J Caleb Snider, Lance A Riley, Noah T Mallory, Matthew R Bersi, Prachi Umbarkar, Rekha Gautam, Qinkun Zhang, Anita Mahadevan-Jansen, Antonis K Hatzopoulos, Luc Maroteaux, et al.

Title: Targeting 5-HT$_{2B}$ Receptor Signaling Prevents Border Zone Expansion and Improves Microstructural Remodeling after Myocardial Infarction.

Authors: J. Caleb Snider[1], Lance A. Riley[1], Noah T. Mallory[1], Matthew R. Bersi[1], Prachi Umbarkar[2], Rekha Gautam[1], Qinkun Zhang[2], Anita Mahadevan-Jansen[1], Antonis K. Hatzopoulos[3], Luc Maroteaux[4], Hind Lal[2], and W. David Merryman[1]*

Affiliations:

[1] Department of Biomedical Engineering, Vanderbilt University, Nashville, TN 37232

[2] Division of Cardiovascular Disease, The University of Alabama at Birmingham, Birmingham, AL 35294

[3] Division of Cardiovascular Medicine, Department of Medicine and Department of Cell and Developmental Biology, Vanderbilt University Medical Center, Nashville, TN 37232

[4] INSERM UMR-S 1270, 75005 Paris, France; Sorbonne Universités, 75005 Paris, France; Institut du Fer à Moulin, 75005 Paris, France

* Address for Correspondence:

W. David Merryman

Room 9445, MRB4

2213 Garland Ave

Nashville, TN 37232

615.322.7219

david.merryman@vanderbilt.edu

Short Title: 5-HT$_{2B}$ in Myocardial Infarction

Total Word Count: 9605 (excluding supplement), **Word Count of Body: 4933**

Abstract

Background: Myocardial infarction (MI) induces an intense injury response which ultimately generates a collagen-dominated scar. While required to prevent ventricular rupture, the fibrotic process is often sustained in a manner detrimental to optimal recovery. Cardiac myofibroblasts are the cells tasked with depositing and remodeling collagen and are a prime target to limit the fibrotic process post-MI. Serotonin 2B receptor (5-HT_{2B}) signaling has been shown to be harmful in a variety of cardiopulmonary pathologies and could play an important role in mediating scar formation after MI.

Methods: We employed two pharmacologic antagonists to explore the effect of 5-HT_{2B} ablation on outcomes post-MI and characterized the histological and microstructural changes involved in tissue remodeling. Inducible, 5-HT_{2B} ablation driven by *Tcf21*^{MCM} and *Postn*^{MCM} were used to evaluate resident cardiac fibroblast- and myofibroblast-specific contributions of 5-$HT_{2B,}$ respectively. RNA sequencing was used to motivate subsequent *in vitro* analyses to explore cardiac fibroblast phenotype.

Results: 5-HT_{2B} antagonism preserved cardiac structure and function by facilitating a less fibrotic scar, indicated by decreased scar thickness and decreased border zone area. 5-HT_{2B} antagonism resulted in collagen fiber redistribution to thinner collagen fibers which were more anisotropic, enhancing left ventricular contractility, while fibrotic tissue stiffness was decreased, limiting the hypertrophic response of uninjured cardiomyocytes. Using a tamoxifen-inducible Cre, we ablated 5-HT_{2B} from *Tcf21*-lineage resident cardiac fibroblasts and saw similar improvements to the pharmacologic approach. Tamoxifen-inducible Cre-mediated ablation of 5-HT_{2B} after onset of injury in *Postn*-lineage myofibroblasts also improved cardiac outcomes. RNA sequencing and subsequent *in vitro* analyses corroborate a decrease in fibroblast

proliferation, migration, and remodeling capabilities through alterations in *Dnajb4* expression and Src phosphorylation.

Conclusions: Together, our findings illustrate that 5-HT_{2B} expression in either cardiac fibroblasts or activated myofibroblasts directly contributes to excessive scar formation, resulting in adverse remodeling and impaired cardiac function after MI.

Keywords: Myocardial infarction, Serotonin 2B receptor, Cardiac fibrosis, Collagen remodeling

Clinical Perspective

What is new?

- Antagonism of the serotonin 2B receptor (5-HT_{2B}) improves outcomes after myocardial infarction through limiting the fibrotic process of scar formation.
- Biomechanical characterization of the scar and adjacent border zone provides useful insight into cardiac fibroblast-mediated fibrosis which results in the associated echocardiographic metrics of tissue structure and function.
- Using pharmacological and genetic approaches, this study pinpoints 5-HT_{2B} expression in myofibroblasts as a regulator of cell proliferation and invasion after myocardial infarction.

What are the clinical implications?

- This study suggests that early inhibition of 5-HT_{2B} signaling after myocardial infarction is sufficient to optimize scar formation, resulting in a functional scar which is less likely to expand beyond the initial infarct and cause long-term remodeling.
- Prolonged presence of the antagonist was not required to maintain the benefits observed in the early stages after injury, indicating that acute treatment can alter chronic remodeling.
- 5-HT_{2B} blockade does not negatively affect any of the vast array of contributors to the healing response after MI provided by non-cardiac fibroblast cell types.

Introduction

Cardiac fibroblasts (CFs) comprise approximately 11% of cells in the healthy adult heart.[1] Quiescent CFs reside in healthy ventricles and maintain homeostasis through low-level extracellular matrix (ECM) turnover and organization.[2,3] Injurious environmental stimuli, such as hypoxia, altered tissue mechanics, and cytokines like TGF-β, signal the phenotypic switch of CFs to a more proliferative, hypercontractile, and hypersecretory state.[4] In the case of myocardial infarction (MI), *Tcf21* lineage-traced resident CFs transdifferentiate into myofibroblasts, which can then be traced through their expression of the marker periostin – a secreted matricellular protein produced in adults exclusively following injury.[5–7] Myofibroblasts localize to both infarcted tissue and the surrounding border zone (BZ) to potentiate the reparative fibrotic injury response due to the lack of intrinsic regenerative capacity of the myocardium.[8–10]

Following MI, myofibroblasts play the indispensable role of stabilizing and reinforcing the left ventricle (LV) via formation of a collagen-dominated scar.[4] Insufficient ECM deposition can lead to LV rupture or aneurysm, while excessive ECM deposition leads to tissue stiffening, scar expansion, and arrhythmias.[11] Furthermore, replacement of contractile myocardium with a collagenous scar creates a local increase in mechanical strain at the BZ of surviving myocardium and scar tissue. To compensate for biomechanical alterations, connective tissue often expands beyond the original injury, creating a subsequent decline in tissue compliance and cardiac output.[12,13] Most chronic myocardial conditions are associated with excessive deposition of fibrotic tissue, making the myofibroblast a desirable therapeutic target to limit fibrotic overactivity.[14,15]

Serotonergic dysfunction has long been understood to contribute to a myriad of cardiopulmonary pathologies. Specifically, signaling through the serotonin 2B receptor (5-HT_{2B})

is particularly involved in valvular heart disease and pulmonary hypertension.[16,17] In response to TGF-β, fibroblast-like valve interstitial cells undergo myofibroblast transformation, which can be prevented with 5-HT_{2B} antagonism.[18] In a murine model of experimental pulmonary hypertension, it has been shown that 5-HT_{2B} in the myeloid compartment is necessary to develop disease and instigate the stiffening of arterioles.[19,20] 5-HT_{2B} has also been shown to play an integral role in mediating isoproterenol-induced cardiac hypertrophy through modulating the inflammatory milieu in a CF-dependent manner.[21] There are multiple downstream 5-HT_{2B} signaling pathways, but the mitogen-activated protein kinase effector p38 and the tyrosine kinase Src are two of the most commonly observed. Both of which are known regulators of cell contractility, ECM deposition, and ECM stiffness.[22,23]

Here, we hypothesized that 5-HT_{2B} antagonism could hinder excessive fibrotic remodeling after MI and create a post-MI scar that preserved cardiac function. We successfully limited adverse remodeling following MI using two independent 5-HT_{2B} antagonists. Using newly developed, tamoxifen-inducible Cre recombinase mouse models for either resident fibroblast- or myofibroblast-targeted ablation of 5-HT_{2B}, we illustrate that CFs have a 5-HT_{2B}-mediated deleterious effect on cardiac structure and function after infarct. We show that targeted ablation of 5-HT_{2B} only from myofibroblasts after injury is sufficient to improve cardiac outcomes. These results are attributed to decreased scar thickness, limited BZ expansion into healthy myocardium, and reduced stiffness of scar tissue. RNA sequencing pointed to a limited proliferative and remodeling capacity in myofibroblasts lacking 5-HT_{2B} driven by an increased expression of *Dnajb4*, which encodes a heat shock protein with known anti-proliferative and anti-invasive properties, and decreased activation of the tyrosine kinase Src.

Methods

The data that support the reported findings and code used for analyses in this study are available from the corresponding author upon reasonable request. All mouse experiments were approved by the Vanderbilt Institutional Animal Care and Use Committee before their commencement. MI was induced via permanent coronary artery occlusion as previously described with consistent infarct size confirmed via TTC staining (Supplemental Figure 1A)[24–26]. Serial echocardiography (example image in Supplemental Figure 1B) was used to assess cardiac structure and function on mice receiving a 5-HT_{2B} antagonist or mice with cell-specific 5-HT_{2B} ablation. *Htr2b*$^{fl/fl}$*Tcf21*$^{MCM/+}$ and *Htr2b*$^{fl/fl}$*Postn*$^{MCM/+}$ mice (inducible resident fibroblast- and myofibroblast-specific 5-HT_{2B} knockouts, respectively) were generated to compare with *Htr2b*$^{fl/fl}$ littermate controls; all mice were crossed with *Rosa26*-stop-tdTomato reporter mice to visually verify Cre activation. Tissue was collected for analysis to determine properties of the scar, BZ, and uninjured myocardium. Picrosirius red staining was used to identify ECM deposition and associated fibrotic measurements (scar thickness, BZ area, and interstitial fibrosis). Polarized light imaging was used to determine collagen fiber thickness and second-harmonic generation imaging to quantify fiber orientation. Atomic force microscopy (AFM) was used to acquire mechanical properties of the tissue and wheat germ agglutinin to identify cardiomyocyte borders for cross-sectional area measurements. CFs (PDGFRα+) were isolated one week after MI from *Htr2b*$^{fl/fl}$ and *Htr2b*$^{fl/fl}$*Postn*$^{MCM/+}$ animals to perform bulk RNA sequencing. CFs were isolated from adult WT and 5-HT_{2B} knockout mice for *in vitro* studies. An expanded methods section is available in the Online Data Supplement.

Results

5-HT$_{2B}$ antagonism preserves cardiac structure and function following MI

To test our hypothesis that 5-HT$_{2B}$ regulates scar formation following MI, we first confirmed there was a marked increase in *Htr2b* expression three days after injury which was sustained into the fibrotic healing phase seven days after infarction (Supplemental Figure 2). *Htr2a,* which encodes the only other member of the 5-HT$_2$ receptor subfamily expressed in the cardiovascular system,[27] is not upregulated until seven days post-MI, and it is still only induced to a fraction of *Htr2b* levels. These findings motivated our exploration into 5-HT$_{2B}$ signaling. To determine if 5-HT$_{2B}$ signaling influences ventricular remodeling after MI, wild-type (WT) mice underwent permanent coronary artery ligation and were administered either vehicle control (dimethyl sulfoxide, DMSO) or the 5-HT$_{2B}$ antagonist SB204741 (SB) at the time of injury (Figure 1A). Interestingly, female mice showed no response to SB treatment (Supplemental Figure 3A-C) which may be due to sex-specific differences of 5-HT$_{2B}$ governed cardiac activity, so subsequent antagonist studies were conducted in male mice.

We observed a preservation of cardiac function indicated by decreased reduction in ejection fraction (EF) and fractional shortening (FS) one week after injury in mice treated with 5-HT$_{2B}$ antagonist, highlighting a slowed LV impairment following MI. This effect was maintained for the six-week period after injury, even with the removal of the antagonist three weeks post-MI (Figure 1B-C). The observed effects were due to the improved systolic inner dimension and volume of the LV (Figure 1D-G). We employed a speckle-tracking algorithm to obtain the global longitudinal strain (GLS) of the LV as another sensitive measure of LV function. While GLS was identically reduced in both groups the first week after injury, cardiac contractility of SB-

treated animals stabilized, while the contractility of DMSO-treated control animals continued to deteriorate over the duration of the experiment (Figure 1H). In order to confirm these results, the experiment was repeated using another selective, high affinity 5-HT_{2B} antagonist RS127445 (RS) which provided a comparable effect (Supplemental figure 4A-H). Heart rate was not affected by inhibition of 5-HT_{2B} signaling (Supplemental Table 1). These data suggest increased 5-HT_{2B} signaling following ischemic injury plays a detrimental role in tissue healing.

Fibrotic injury response is altered by 5-HT_{2B} antagonism

Using a custom-built image processing pipeline,[4] short-axis tissue sections were analyzed six weeks following MI (unless otherwise noted) to identify the role of 5-HT_{2B} signaling in the healing process post-MI. Tissue thickness was calculated and picrosirius red staining demarcated the viable myocardium (yellow) from collagenous scar tissue (red; Figure 2A-B). The BZ (green dots; Figure 2B) was defined as the transition region between collagen-dominated scar tissue (stained >85% red) and myocardium-dominated tissue (stained >85% yellow) (Figure 2C). In SB-treated mice, the deposition of fibrotic tissue was diminished as indicated by the formation of a thinner scar than control mice (Figure 2D). Scars in the SB-treated group appear to form thinner in the first week after injury and retain this thinness from week one to week six. This composition did not compromise scar integrity as there was no difference in mortality between the two groups (Supplemental Figure 5).

We then calculated the BZ transition rate (indicated by the slope of the green dot region plotted in Figure 2C) to quantify the area of material mismatch between the contractile myocardium and stiff, collagenous scar. We observed an increased rate of change from collagen

to myocardium (i.e. a shorter BZ region) with 5-HT_{2B} antagonism revealing decreased BZ infiltration and scar disruption of viable myocardium (Figure 2E). There were no differences in the area fraction of collagen in the remote uninjured myocardium to indicate tissue-wide fibrosis (Figure 2F).

Since we observed differences in fibrotic response in both the scar and BZ of SB-treated animals, picrosirius red staining was imaged under polarized light to observe collagen fiber thickness. While there was no shift in the distribution of collagen fiber thickness in the scar, a higher percentage of thin collagen fibers was observed in response to 5-HT_{2B} antagonism within the BZ (Figure 2G-H). We also used second-harmonic generation (SHG) imaging to analyze collagen fiber orientation (Supplemental Figure 6). SB-treated mice had a higher fraction of fields of view (FOV) dominated by strongly aligned, anisotropic collagen fibers in the BZ, which would impart an improved contractility (Figure 2I). Mice treated with RS also demonstrated similar alterations in the scar formation process (Supplemental Figure 7A-C). Histological analyses indicate that treatment with a 5-HT_{2B} antagonist is capable of controlling scar formation after MI and limiting BZ expansion through alterations in collagen fiber formation and organization.

Microstructural changes in response to impaired 5-HT_{2B} signaling

We next explored how alterations in the fibrotic healing process affects tissue stiffness. AFM was used to investigate mechanical changes of the fibrotic tissue area to determine if tissue compliance could play a role in preserving cardiac function in response to SB treatment. While there were no differences in tissue stiffness in the early stages of scar formation, antagonist-

treated groups showed a decreased tissue stiffness in both the scar and BZ at six weeks following injury (Figure 3A-B, Supplemental Figure 7D). There were no changes in the myocardial stiffness in uninjured myocardium (Supplemental Figure 8).

Since increased tissue stiffening can lead to a hypertrophic response in cardiomyocytes,[28] we quantified the expression of the gene encoding the cardiomyocyte injury marker natriuretic peptide B (*Nppb*). Six weeks after MI, there was a significant reduction in *Nppb* in the SB group (Figure 3C). To further characterize the cardiomyocyte response to diminished fibrotic remodeling, short-axis cross-sectional area of cardiomyocytes distant to the infarcted tissue was quantified. We observed a significant increase in cardiomyocyte area six weeks after MI in vehicle treated animals compared to SB-treated animals (Figure 3D-E); these results again held with RS treatment (Supplemental Figure 7E). There was also a significant increase in cardiomyocyte area of vehicle-treated animals over their sham counterparts which was prevented with SB treatment (Figure 3E). These results indicate a biophysical alteration in cardiac composition downstream of the scar formation process influences remote cardiomyocyte hypertrophy after MI.

Deletion of 5-HT_{2B} in resident fibroblasts improves cardiac response to MI

We next examined potential cell populations responsible for the effects seen following systemic administration of a 5-HT_{2B} antagonist. While it is known 5-HT_{2B} influences cardiomyocyte development and mitogenesis,[29,30] we did not observe alterations in cardiac structure or function in sham-operated animals given antagonist (Supplemental Figure 9A-C). Therefore, we ruled out that 5-HT_{2B} antagonism in the absence of injury affects the resident cell

populations (primarily cardiomyocytes) with regards to LV dimensions or output. In the context of MI, we investigated *Htr2b* expression via quantitative polymerase chain reaction (qPCR) in three cell populations. First, adult cardiomyocytes were isolated from infarcted LVs seven days after injury. Compared to sham operation, there was approximately a 5-fold increase in *Htr2b* expression (Supplemental Figure 10A). However, since we observed an 17-fold increase in bulk tissue at this time point (Supplemental Figure 2), we sought other contributing cell types. The next cell population investigated was endothelial cells. WT mice were subjected to MI, and CD31-expressing cells were isolated via fluorescence-activated cell sorting (FACS). qPCR revealed that CD31+ cells had a negligible contribution to the 17-fold induction of *Htr2b* following MI (Supplemental Figure 10B-C). Furthermore, there was not an alteration in the expression for the gene encoding E-selectin (*Sele*) in scar tissue of mice treated with a 5-HT_{2B} antagonist, indicating blocking 5-HT_{2B} signaling does not mediate endothelial cell activation (Supplemental Figure 10E). While there was no increase in *Htr2b* expression in CD45+ cells seven days after MI compared to sham operation (Supplemental Figure 10B,D), there was the possibility that the immune cells, which infiltrate early after injury, had already been cleared from the injury. To test this hypothesis, we used a bone marrow transplant model based on previous findings showing that mice lacking 5-HT_{2B} in the bone marrow compartment exhibit decreased tissue remodeling and arteriole stiffness in an experimental model of pulmonary hypertension.[19,20] Age- and sex-matched donors (WT or *Htr2b*$^{-/-}$) were transplanted into WT mice with engraftment success of approximately 95% (Supplemental Figure 11A-B). We observed no differences in cardiac structure or function between the transplant groups after MI, indicating a cell type of non-hematopoietic origin mediated the results observed in the 5-HT_{2B} antagonist studies (Supplemental Figure 12A-D).

To determine if 5-HT_{2B} signaling in the remaining major cardiac cell population, resident CFs, impacts healing after MI, we deleted the gene encoding 5-HT_{2B} in resident CFs using a tamoxifen-inducible, *Tcf21*^{MerCreMer} (*Tcf21*^{MCM}) transgene[7,31] (Figure 4A). The tdTomato fluorescent reporter was observed in all *Htr2b*$^{fl/fl}$*Tcf21*$^{MCM/+}$ mice indicating successful recombination in the CFs without affecting survival (Supplemental Figure 13A-B, Supplemental Figure 14A). Following MI, *Htr2b*$^{fl/fl}$*Tcf21*$^{MCM/+}$ mice exhibited significantly improved EF and FS (Figure 4B-C). These mice also had preserved LV inner dimension and volume in both diastole and systole six weeks post-MI (Figure 4D-G). GLS steadily decreased over time in *Htr2b*$^{fl/fl}$ mice lacking the *Tcf21*^{MCM} transgene and was significantly lower than the stabilized contractility of mice harboring the *Tcf21*^{MCM} transgene (Figure 4H). Six weeks after MI, morphometric analysis revealed increased heart weight to tibia length in *Htr2b*$^{fl/fl}$ mice indicative of cardiac hypertrophy (Figure 4I). These results show that ablation of the 5-HT_{2B} receptor from resident CFs is effective in improving cardiac outcomes after MI in a manner similar to that achieved with 5-HT_{2B} antagonism.

Myofibroblast-specific deletion of 5-HT_{2B} improves cardiac response to MI

Tcf21^{MCM} driven ablation of 5-HT_{2B} targets residential CFs present even in the absence of injury. We wanted to assess the functionality of ablating 5-HT_{2B} after the induction of an MI. We utilized a mouse model which expressed the MCM cDNA driven by the periostin promoter (*Postn*^{MCM}) (Figure 5A). This mouse model has been well-characterized to demonstrate the marking of nearly all newly activated fibroblasts (myofibroblasts) following an injury, without induction prior to injury.[6,32] Following MI, all *Htr2b*$^{fl/fl}$*Postn*$^{MCM/+}$ hearts exhibited signal from

the tdTomato reporter, indicating successful recombination without affecting survival (Supplemental Figure 14B, Supplemental Figure 15). *Htr2b*$^{fl/fl}$*Postn*$^{MCM/+}$ mice demonstrated a significant improvement in the functional metrics of EF and FS one week after MI compared to *Htr2b*$^{fl/fl}$ animals which were maintained six weeks following the injury (Figure 5B-C). Myofibroblast-specific 5-HT_{2B} ablation resulted in improved LV inner dimension and volume in both diastole and systole six weeks after MI, indicating a preserved cardiac structure (Figure 5D-G). Ventricular deformation measured by GLS was preserved in the *Htr2b*$^{fl/fl}$*Postn*$^{MCM/+}$ group while the control group continued to deteriorate over the six-week experiment (Figure 5H). Finally, morphometric analyses revealed a decreased heart weight with 5-HT_{2B} ablation (Figure 5I). As it has been shown that tissue-resident fibroblasts of the *Tcf21* lineage are the primary source of subsequent injury-activated, periostin-expressing myofibroblasts [6], these results confirm 5-HT_{2B} expression in the CF population worsens the injury response to MI and that blocking 5-HT_{2B} signaling after injury is sufficient to improve cardiac outcomes.

5-HT_{2B} knockout decreases CF proliferative and remodeling capacity

In order to investigate how periostin-driven ablation of 5-HT_{2B} imparts beneficial outcomes following MI, we performed RNA sequencing on PDGFRα+ cells isolated via FACS from the scar tissue of infarcted hearts seven days after MI (Supplemental Figure 16A-B). Despite only about 20% of PDGFRα+ cells being tdTomato+ in the *Htr2b*$^{fl/fl}$*Postn*$^{MCM/+}$ group (indicating 5-HT_{2B} knockout), we observed differential expression of 63 genes which, following Gene Ontology (GO) analysis, were overwhelmingly associated with biological processes linked to the control of cell cycle and mitosis as well as individual genes (i.e. *Nexn*, *Robo4*, *Fgf23*, and

Arhgap5) governing cell migration and remodeling (Figure 6A, Supplemental Table 2). One such gene of interest that was upregulated in the $Htr2b^{fl/fl}Postn^{MCM/+}$ group was the tumor suppressor *Dnajb4* which reduces the invasive and metastatic behavior cellular phenotype in lung cancer.[33,34] In isolated 5-$HT_{2B}^{-/-}$ CFs, it was observed that loss of 5-HT_{2B} resulted in an increased expression of *Dnajb4* (Figure 6B). As previous reports have shown *Dnajb4* controls the activation of Src[33], we probed Src phosphorylation in CFs and observed a decreased phosphorylation of Src in 5-$HT_{2B}^{-/-}$ CFs (Figure 6C, Supplemental Figure 17). The decrease in these molecular mediators of cell proliferation and invasion led us to investigate the capabilities of CFs to populate the wounded tissue after MI. We observed a decreased area fraction of periostin staining in the infarct of SB-treated mice one week after injury, indicative of decreased myofibroblast proliferation and infiltration (Figure 6D). Similarly, *in vitro* analysis of 5-$HT_{2B}^{-/-}$ CFs revealed a decreased proliferative capacity as seen by fewer cells incorporating BrdU (Figure 6E). CFs lacking 5-HT_{2B} demonstrated an approximate 50% decrease in migratory capacity in an *in vitro* wound healing assay (Figure 6F). Finally, CFs were seeded into free-floating collagen gels in order to test their ability to remodel a collagen matrix. In gels seeded with 5-$HT_{2B}^{-/-}$ CFs, gel contraction after 72 hours was significantly hindered (Figure 6G). These results point to a mechanism of 5-HT_{2B}-mediated myofibroblast proliferation and matrix remodeling leading to adverse scar formation following MI.

Discussion

Experimental MI induced by permanent coronary artery occlusion triggers the expansion and activation of resident CFs from their quiescent, homeostatic state. CFs transdifferentiate into highly active myofibroblasts following injury, migrating to and proliferating at the site of tissue

damage to secrete ECM and contract scar tissue.[35,36] The quality of initial scar formation has lasting effects on cardiac outcomes. A structurally sufficient scar is necessary to reinforce the LV wall, but persistent fibrotic activity leads to chronic cardiac deterioration.[11,37] Therefore, it is desirable to properly tune the fibrotic response following MI such that a functional scar is able to form but is dampened before the activity of myofibroblasts becomes deleterious.

Prior studies have shown anti-fibrotic effects of 5-HT_{2B} disruption in various cardiopulmonary pathologies.[19–21,38,39] To our knowledge, this study is the first investigation to report the direct contribution of 5-HT_{2B} signaling in wound healing after MI. Through the implementation of two pharmacological inhibitors and two models of genetically targeted ablation, we have shown that the 5-HT_{2B} receptor is an effective target to limit fibrosis following MI injury in mice. Due to advances in identification of genetic markers for CFs, we were able to isolate myofibroblasts as the cell population responsible for the improved recovery after MI seen in animals treated with a 5-HT_{2B} antagonist.

In the present study, echocardiographic analysis revealed global 5-HT_{2B} antagonism improves cardiac structure and function one week after MI versus vehicle treatment. While there were not significant changes in these metrics between one and six weeks after injury, GLS deteriorated from week one to six in the control groups whereas 5-HT_{2B} inhibition stabilized this measure of cardiac contractility. GLS has been shown to be an independent predictor of adverse remodeling after ST-elevated MI in humans and can be a more sensitive functional output than the traditionally used EF.[40]

We further explored changes to tissue architecture which led to an improvement in cardiac function and alterations in scar formation. A heavier collagen burden increases passive tissue stiffness, heightening afterload and hindering systolic function.[41] 5-HT_{2B} blockade

successfully decreased collagen burden, indicated by decreased scar thickness, without negatively affecting survival rate. The BZ is a vulnerable region of tissue which experiences heightened wall stress and where scar expansion occurs, further damaging cardiomyocytes not directly affected by the initial ischemic event.[13,42] We found that targeting 5-HT_{2B} resulted in an increased transition rate from scar tissue to surviving myocardium (i.e. less BZ region), revealing decreased intrusion of collagen fibers from the scar into uninjured myocardium. The prevention of scar expansion can minimize the disruption of the cardiac syncytium, providing a more coordinated systolic cycle.[43] Similar to reports linking 5-HT_{2B} to collagen content and composition through activation of lung and valve fibroblasts, [38,44] our results show a redistribution of collagen fiber thickness in the BZ, favoring less mature, more compliant collagen fibers. This difference was not seen in the scar, further suggesting the formation of a mechanically sound scar with limited capacity to expand beyond the BZ. The collagen fibers in BZs of SB-treated animals exhibited more frequent regions of anisotropic collagen fiber distributions which are able to undergo elastic deformation along with cardiomyocyte contraction and increase LV contraction.[45] This effect is enhanced by the softer scar and BZ. Since these effects prevented early hypertrophic signs observed in control animals, 5-HT_{2B} antagonism reveals a desirable mechanical and biophysical outcome after MI achieved by a muted initial fibrotic response that provides adequate scar formation without hindering the systolic capabilities of the heart.

It is clear that the translational approach of pharmacological inhibition of 5-HT_{2B} signaling is effective to establish a therapeutic effect on scar formation and gives insight into the mechanistic alterations of collagen deposition and remodeling, but the lack of specificity renders it insufficient to identify the cell population which mediates the observed effect. Therefore, we

implemented several models to manipulate 5-HT_{2B} in different cell populations. Cardiomyocytes express 5-HT_{2B}, and blockade of this receptor can partially mitigate noradrenaline overload-induced hypertrophy.[46] Cardiomyocytes isolated seven days after infarct do show an increase in *Htr2b* expression, but only to a fraction of the degree to which expression is increased in bulk tissue. CD31+ cells neither exhibited increased *Htr2b* gene expression after infarct nor altered gene expression for the marker of endothelial activation, E-selectin. Similarly, *Htr2b* expression in CD45+ cells did not change after MI, and bone-marrow transplants from 5-HT_{2B}-knockout mice did not recapitulate the results from antagonist studies, pointing to a mechanism different from previous reports exploring fibrotic remodeling in pulmonary disease.[19,20] Therefore, we developed a novel model of CF-specific 5-HT_{2B} ablation using *Tcf21*-driven Cre expression. This approach circumvented developmental defects seen with gestational ablation of 5-HT_{2B};[30] however, it could also have imparted benefits prior to MI. Regardless, eliminating 5-HT_{2B} from resident, *Tcf21*-expressing CFs resulted in a vastly improved cardiac phenotype compared to control animals. Similar improvements as the antagonist studies were achieved with even more pronounced structural benefits observed in the improvement in both LV systolic and diastolic metrics, as well as a decreased heart weight. The enhanced effects of the genetic approach over the pharmacological approach are most likely due to a sufficient recombination of the *Htr2b* gene locus to convey a stronger effect than what is achieved by transient binding of the antagonist which is subject to metabolic processing and removal from the system.

To implement an approach which more closely replicates the pharmacological strategy, we utilized a *Postn*-driven model of 5-HT_{2B} ablation. Myofibroblasts, which are overwhelmingly derived from a *Tcf21* lineage,[6] are absent in healthy tissue and populate the infarct zone 2-4 days after injury.[14] Targeting this specialized cell type achieved nearly identical results as the *Tcf21*-

driven model and further hones in on the population affected by 5-HT_{2B} antagonism. Knowing that myofibroblasts are derived from resident fibroblasts, the overlapping results importantly demonstrate that targeting injury-responsive myofibroblasts without affecting their progenitor cells is sufficient to affect scar formation after MI. The mechanistic implication of this result is that 5-HT_{2B}-dependent infiltration and scar remodeling occurs after the transdifferentiation of resident CFs. Furthermore, it demonstrates the redundancy in the two genetic models where targeting either resident CFs in the absence of injury or myofibroblasts derived from resident CFs achieves the same result.

While only the contribution of bone marrow-derived populations was explicitly eliminated, initial evidence reveals that the contribution of cardiomyocyte or endothelial expression of 5-HT_{2B} plays a negligible role in improving scar formation after MI. We reported a dramatic increase in *Htr2b* expression after MI which cannot be accounted for by cardiomyocytes, CD31+, and/or CD45+ cells. Considering the utility of the CF-specific genetic ablation of 5-HT_{2B}, we are confident that this increase is due to CFs. Pericytes cannot be excluded as potential contributors as these cells express *Tcf21* and function in a multiplicity of roles involved in MI healing.[7,9,47] The periostin-driven model of 5-HT_{2B} ablation in myofibroblasts should circumvent pericyte contribution, and so we are confident that cells which produce and organize collagen are the primary effector cells. While cardiomyocyte expression of *Htr2b* is increased after MI, it accounts for a small fraction of the total increase. In healthy hearts, cardiomyocytes are bountiful with CFs making up a small portion of cells.[1] While these populations shift after injury, it is still conceivable that the contribution of cardiomyocyte 5-HT_{2B} is minimal since a more abundant cell population is a minor contributor with mesenchymal cells accounting for the vast majority of *Htr2b* expression. In addition, reports show blocking 5-HT_{2B}

signaling after injury may reduce cardiomyocyte hypertrophy,[46,48] providing additional protection in the antagonist studies. Regardless, cardiomyocyte expression of 5-HT_{2B} is intact with the *Tcf21*- and *Postn*-driven 5-HT_{2B} ablation models, further supporting that the alteration in scar formation and cardiac outcomes is mediated by a fibroblast cell population. Because of this evidence, utilization of 5-HT_{2B} antagonists provides an approach to further investigate the mechanism behind improved cardiac outcomes. Since myofibroblasts are not immediately present after MI, it may not be necessary to begin treatment instantly after injury. Furthermore, since echocardiographic readouts were improved as early as seven days after injury, it is possible that 5-HT_{2B} inhibition during the acute healing phase of initial scar formation is sufficient to preserve cardiac performance.

It is interesting that 5-HT_{2B} antagonism was ineffective in females. It has been shown that global knockout of 5-HT_{2B} results in more severe histopathological lesions and a stronger systolic dysfunction in adult male mice compared to females as a result of impaired cardiac development.[30] Furthermore, sex-specific differences in hepatocellular carcinoma has been attributed to increased serotonin production in males compared to females, resulting in a 5-HT_{2B}-mediated increase of fibrogenic hepatic stellate cells density.[49] It must be noted that both males and females were included in both genetic models, and both sexes responded similarly to 5-HT_{2B} ablation. While genetic manipulation is sufficient to improve outcomes in females, these observations indicate that there is a biological difference in the way that female mice respond to 5-HT_{2B} antagonism, potentially through metabolic processing of the molecule or ligand/receptor interactions.

RNA sequencing revealed 5-HT_{2B} as a regulator of proliferation and matrix remodeling in CFs. We employed a surrogate CF marker PDGFRα[50] to select for CFs, and despite only 20% of

these cells displaying the tdTomato fluorescent reporter in the *Htr2b*$^{fl/fl}$*Postn*$^{MCM/+}$ group, we still observed differential regulation of multiple genes in myofibroblasts with 5-HT$_{2B}$ ablation. Supported by differences in associated GO terms, we primarily investigated CF proliferation as well as ECM remodeling. We saw upregulation of genes such as *Plagl1* which inhibits cell growth and proliferation, potentially through PPARγ,[51] and *Nexn* whose loss is associated with dilated cardiomyopathy.[52] Several interesting transcripts were also downregulated: *Lrp2* which increases proliferation of epicardial cells (CF precursors),[53] *Fgf23* which demonstrates broad mitogenic and cell survival actions specifically in the heart,[54] and *Robo4* which is associated with increased matrix metalloproteinase expression and predisposition for aortic valve disease.[55] Of note, we have shown that in CFs lacking 5-HT$_{2B}$, *Dnajb4* is upregulated. It is known that the heat shock protein encoded by this gene is highly expressed in human CFs.[56] There is a direct link to increased expression of this protein and the inhibition of Src,[33] and consistent with this prior report, we found decreased phosphorylation of Src in 5-HT$_{2B}^{-/-}$ CFs. *Dnajb4* is known to control cell proliferation and migration, supporting our observations in which myofibroblasts were sparser in damaged tissue of SB-treated animals and 5-HT$_{2B}$ knockout decreasing proliferation, migration, and collagen matrix remodeling. The known link between *Dnajb4*, Src phosphorylation, and cell proliferation and remodeling capacity provides a mechanistic insight into the improved phenotype observed with 5-HT$_{2B}$ inhibition. Blocking 5-HT$_{2B}$ signal transduction in the beginning stages of scar formation hinders the proliferation and migration of myofibroblasts into the infarct zone through increasing *Dnajb4* expression, which, in turn, inhibits endogenous activation of Src. This approach allowed myofibroblasts to form a functional scar while avoiding a mechanical environment that predisposes the tissue to scar expansion and hypertrophy.

Due to the complexities associated with the intricate coordination involved in the inflammatory response post-MI, we set out to target the effector cells of fibrosis (i.e. CFs) to control the initial reparative response and limit adverse fibrotic remodeling. Targeting 5-HT_{2B} on CFs can control scar mechanics and limit fibrosis without affecting scar stability.[57] Further, inhibiting the activity of 5-HT_{2B} has an acute benefit that is sustained well beyond the initial healing phase and demonstrates that cardiac hypertrophy subsequent to an ischemic event can be curtailed. Taken together, this work has identified 5-HT_{2B} as a potential therapeutic target for muting the over activity of myofibroblasts following MI to preserve cardiac phenotype and prevent the initiation and progression of cardiac fibrosis and heart failure.

Sources of Funding

This work was supported by the National Institutes of Health: R35-HL135790 (WDM), R01-HL115103 (WDM), R01-HL133290 (HL), R01-HL143074 (HL), R01-HL138519 (AKH), K99-HL146951 (MRB), F32- HL154596 (LAR), T32-HL007411 (MRB), T32-EB021937 (LAR); American Heart Association: 18PRE34060078 (JCS); and a grant from the Fondation Leducq.

Acknowledgements

We thank Dr. Lin Zhong in the Cardiovascular Physiology Core for performing all of the echocardiography and Vanderbilt Technologies for Advanced Genomics (VANTAGE) for performing RNA sequencing. We thank Dr. Michelle Tallquist and Dr. Jeffery Molkentin for providing the *Tcf21*^{MCM} and *Postn*^{MCM} animals, respectively.

Disclosures

None.

References

1. Pinto AR, Ilinykh A, Ivey MJ, Kuwabara JT, D'Antoni ML, Debuque R, et al. Revisiting Cardiac Cellular Composition. *Circ Res* 2016;118:400–409. doi: 10.1161/CIRCRESAHA.115.307778.
2. Valiente-Alandi I, Potter SJ, Salvador AM, Schafer AE, Schips T, Carrillo-Salinas F, et al. Inhibiting Fibronectin Attenuates Fibrosis and Improves Cardiac Function in a Model of Heart Failure. *Circulation* 2018;138:1236–1252. doi: 10.1161/CIRCULATIONAHA.118.034609.
3. Nagaraju CK, Dries E, Popovic N, Singh AA, Haemers P, Roderick HL, et al. Global fibroblast activation throughout the left ventricle but localized fibrosis after myocardial infarction. *Sci Reports 2017 71* 2017;7:10801. doi: 10.1038/s41598-017-09790-1.
4. Schroer AK, Bersi MR, Clark CR, Zhang Q, Sanders LH, Hatzopoulos AK, et al. Cadherin-11 blockade reduces inflammation-driven fibrotic remodeling and improves outcomes after myocardial infarction. *JCI Insight* 2019;4. doi: 10.1172/jci.insight.131545.
5. Snider P, Standley KN, Wang J, Azhar M, Doetschman T, Conway SJ. Origin of cardiac fibroblasts and the role of periostin. *Circ Res* 2009;105:934–947. doi: 10.1161/CIRCRESAHA.109.201400.
6. Kanisicak O, Khalil H, Ivey MJ, Karch J, Maliken BD, Correll RN, et al. Genetic lineage tracing defines myofibroblast origin and function in the injured heart. *Nat Commun*

2016;7:12260. doi: 10.1038/ncomms12260.

7. Acharya A, Baek ST, Huang G, Eskiocak B, Goetsch S, Sung CY, et al. The bHLH transcription factor Tcf21 is required for lineage-specific EMT of cardiac fibroblast progenitors. *Development* 2012;139:2139–2149. doi: 10.1242/dev.079970.

8. Chistiakov DA, Orekhov AN, Bobryshev Y V. The role of cardiac fibroblasts in post-myocardial heart tissue repair. *Exp Mol Pathol* 2016;101:231–240. doi: 10.1016/J.YEXMP.2016.09.002.

9. Prabhu SD, Frangogiannis NG. The Biological Basis for Cardiac Repair After Myocardial Infarction: From Inflammation to Fibrosis. *Circ Res* 2016;119:91–112. doi: 10.1161/CIRCRESAHA.116.303577.

10. Paik DT, Rai M, Ryzhov S, Sanders LN, Aisagbonhi O, Funke MJ, et al. Wnt10b gain-of-function improves cardiac repair by arteriole formation and attenuation of fibrosis. *Circ Res* 2015;117:804–816. doi: 10.1161/CIRCRESAHA.115.306886.

11. Daseke MJ, Tenkorang MAA, Chalise U, Konfrst SR, Lindsey ML. Cardiac fibroblast activation during myocardial infarction wound healing. *Matrix Biol* 2020;91–92:109–116. doi: 10.1016/j.matbio.2020.03.010.

12. Talman V, Ruskoaho H. Cardiac fibrosis in myocardial infarction—from repair and remodeling to regeneration. *Cell Tissue Res* 2016;365:563–581. doi: 10.1007/s00441-016-2431-9.

13. Jackson BM, Gorman JH, Salgo IS, Moainie SL, Plappert T, St. John-Sutton M, et al. Border zone geometry increases wall stress after myocardial infarction: contrast echocardiographic assessment. *Am J Physiol Circ Physiol* 2003;284:H475–H479. doi: 10.1152/ajpheart.00360.2002.

14. Humeres C, Frangogiannis NG. Fibroblasts in the Infarcted, Remodeling, and Failing Heart. *JACC Basic to Transl Sci* 2019;4:449–467. doi: 10.1016/j.jacbts.2019.02.006.
15. van Putten S, Shafieyan Y, Hinz B. Mechanical control of cardiac myofibroblasts. *J Mol Cell Cardiol* 2016;93:133–142. doi: 10.1016/j.yjmcc.2015.11.025.
16. Rothman RB, Baumann MH, Savage JE, Rauser L, McBride A, Hufeisen SJ, et al. Evidence for Possible Involvement of 5-HT $_{2B}$ Receptors in the Cardiac Valvulopathy Associated With Fenfluramine and Other Serotonergic Medications. *Circulation* 2000;102:2836–2841. doi: 10.1161/01.CIR.102.23.2836.
17. Launay J-M, Hervé P, Peoc'h K, Tournois C, Callebert J, Nebigil CG, et al. Function of the serotonin 5-hydroxytryptamine 2B receptor in pulmonary hypertension. *Nat Med* 2002;8:1129–1135. doi: 10.1038/nm764.
18. Hutcheson JD, Ryzhova LM, Setola V, Merryman WD. 5-HT(2B) antagonism arrests non-canonical TGF-β1-induced valvular myofibroblast differentiation. *J Mol Cell Cardiol* 2012;53:707–714. doi: 10.1016/j.yjmcc.2012.08.012.
19. Launay J-M, Hervé P, Callebert J, Mallat Z, Collet C, Doly S, et al. Serotonin 5-HT2B receptors are required for bone-marrow contribution to pulmonary arterial hypertension. *Blood* 2012;119.
20. Bloodworth NC, Clark CR, West JD, Snider JC, Gaskill C, Shay S, et al. Bone Marrow–Derived Proangiogenic Cells Mediate Pulmonary Arteriole Stiffening via Serotonin 2B Receptor Dependent Mechanism. *Circ Res* 2018;123:e51–e64. doi: 10.1161/CIRCRESAHA.118.313397.
21. Jaffré F, Bonnin P, Callebert J, Debbabi H, Setola V, Doly S, et al. Serotonin and angiotensin receptors in cardiac fibroblasts coregulate adrenergic-dependent cardiac

hypertrophy. *Circ Res* 2009;104:113–123. doi: 10.1161/CIRCRESAHA.108.180976.

22. He L, Huang X, Kanisicak O, Li Y, Wang Y, Li Y, et al. Preexisting endothelial cells mediate cardiac neovascularization after injury. *J Clin Invest* 2017;127:2968–2981. doi: 10.1172/JCI93868.

23. West JD, Carrier EJ, Bloodworth NC, Schroer AK, Chen P, Ryzhova LM, et al. Serotonin 2B Receptor Antagonism Prevents Heritable Pulmonary Arterial Hypertension. *PLoS One* 2016;11:e0148657. doi: 10.1371/journal.pone.0148657.

24. Gao E, Lei YH, Shang X, Huang ZM, Zuo L, Boucher M, et al. A Novel and Efficient Model of Coronary Artery Ligation and Myocardial Infarction in the Mouse. *Circ Res* 2010;107:1445–1453. doi: 10.1161/CIRCRESAHA.110.223925.

25. Wu L, Dalal R, Cao CD, Postoak JL, Yang G, Zhang Q, et al. IL-10–producing B cells are enriched in murine pericardial adipose tissues and ameliorate the outcome of acute myocardial infarction. *Proc Natl Acad Sci U S A* 2019;116:21673–21684. doi: 10.1073/pnas.1911464116.

26. Lal H, Ahmad F, Zhou J, Yu JE, Vagnozzi RJ, Guo Y, et al. Cardiac fibroblast glycogen synthase kinase-3β regulates ventricular remodeling and dysfunction in ischemic heart. *Circulation* 2014;130:419–430. doi: 10.1161/CIRCULATIONAHA.113.008364.

27. Maroteaux L, Ayme-Dietrich E, Aubertin-Kirch G, Banas S, Quentin E, Lawson R, et al. New therapeutic opportunities for 5-HT2 receptor ligands. *Pharmacol Ther* 2017;170:14–36. doi: 10.1016/j.pharmthera.2016.10.008.

28. Schelbert EB, Butler J, Diez J. Why Clinicians Should Care About the Cardiac Interstitium. *JACC Cardiovasc Imaging* 2019;12:2305–2318. doi: 10.1016/j.jcmg.2019.04.025.

29. Nebigil CG, Choi DS, Dierich A, Hickel P, Le Meur M, Messaddeq N, et al. Serotonin 2B receptor is required for heart development. *Proc Natl Acad Sci U S A* 2000;97:9508–9513. doi: 10.1073/pnas.97.17.9508.

30. Nebigil CG, Hickel P, Messaddeq N, Vonesch JL, Douchet MP, Monassier L, et al. Ablation of serotonin 5-HT(2B) receptors in mice leads to abnormal cardiac structure and function. *Circulation* 2001;103:2973–2979. doi: 10.1161/01.cir.103.24.2973.

31. Acharya A, Baek ST, Banfi S, Eskiocak B, Tallquist MD. Efficient inducible Cre-mediated recombination in Tcf21cell lineages in the heart and kidney. *Genesis* 2011;49:870–877. doi: 10.1002/dvg.20750.

32. Molkentin JD, Bugg D, Ghearing N, Dorn LE, Kim P, Sargent MA, et al. Fibroblast-Specific Genetic Manipulation of p38 Mitogen-Activated Protein Kinase In Vivo Reveals Its Central Regulatory Role in Fibrosis. *Circulation* 2017;136:549–561. doi: 10.1161/CIRCULATIONAHA.116.026238.

33. Chen CH, Chang WH, Su KY, Ku WH, Chang GC, Hong QS, et al. HLJ1 is an endogenous Src inhibitor suppressing cancer progression through dual mechanisms. *Oncogene* 2016;35:5674–5685. doi: 10.1038/onc.2016.106.

34. Wang CC, Tsai MF, Dai TH, Hong TM, Chan WK, Chen JJW, et al. Synergistic activation of the tumor suppressor, HLJ1, by the transcription factors YY1 and activator protein 1. *Cancer Res* 2007;67:4816–4826. doi: 10.1158/0008-5472.CAN-07-0504.

35. Driesen RB, Nagaraju CK, Abi-Char J, Coenen T, Lijnen PJ, Fagard RH, et al. Reversible and irreversible differentiation of cardiac fibroblasts. *Cardiovasc Res* 2014;101:411–422. doi: 10.1093/cvr/cvt338.

36. Herum KM, Choppe J, Kumar A, Engler AJ, McCulloch AD. Mechanical regulation of

cardiac fibroblast profibrotic phenotypes. *Mol Biol Cell* 2017;28:1871–1882. doi: 10.1091/mbc.e17-01-0014.

37. Li L, Zhao Q, Kong W. Extracellular matrix remodeling and cardiac fibrosis. *Matrix Biol* 2018;68–69:490–506. doi: 10.1016/J.MATBIO.2018.01.013.

38. Driesbaugh KH, Branchetti E, Grau JB, Keeney SJ, Glass K, Oyama MA, et al. Serotonin receptor 2B signaling with interstitial cell activation and leaflet remodeling in degenerative mitral regurgitation. *J Mol Cell Cardiol* 2018;115:94–103. doi: 10.1016/j.yjmcc.2017.12.014.

39. Janssen W, Schymura Y, Novoyatleva T, Kojonazarov B, Boehm M, Wietelmann A, et al. 5-HT2B Receptor Antagonists Inhibit Fibrosis and Protect from RV Heart Failure. *Biomed Res Int* 2015;2015:1–8. doi: 10.1155/2015/438403.

40. Reindl M, Tiller C, Holzknecht M, Lechner I, Eisner D, Riepl L, et al. Global longitudinal strain by feature tracking for optimized prediction of adverse remodeling after ST-elevation myocardial infarction. *Clin Res Cardiol* 2020:1–11. doi: 10.1007/s00392-020-01649-2.

41. Gonzalez A, Lopez B, Ravassa S, San Jose G, Diez J. The complex dynamics of myocardial interstitial fibrosis in heart failure. Focus on collagen cross-linking. *BBA - Mol Cell Res* 2019;1866:1421–1432. doi: https://doi.org/10.1016/j.bbamcr.2019.06.001.

42. Dick SA, Macklin JA, Nejat S, Momen A, Clemente-Casares X, Althagafi MG, et al. Self-renewing resident cardiac macrophages limit adverse remodeling following myocardial infarction. *Nat Immunol* 2019;20:29–39. doi: 10.1038/s41590-018-0272-2.

43. Weber KT, Sun Y, Bhattacharya SK, Ahokas RA, Gerling IC. Myofibroblast-mediated mechanisms of pathological remodelling of the heart. *Nat Rev Cardiol* 2013;10:15–26.

doi: 10.1038/nrcardio.2012.158.

44. Fabre A, Marchal-Sommé J, Marchand-Adam S, Quesnel C, Borie R, Dehoux M, et al. Modulation of bleomycin-induced lung fibrosis by serotonin receptor antagonists in mice. *Eur Respir J* 2008;32:426–436. doi: 10.1183/09031936.00126907.

45. Holmes JW, Laksman Z, Gepstein L, Holmes J. Making Better Scar: Emerging Approaches for Modifying Mechanical and Electrical Properties Following Infarction and Ablation HHS Public Access. *Prog Biophys Mol Biol Prog Biophys Mol Biol* 2016;120:134–148. doi: 10.1016/j.pbiomolbio.2015.11.002.

46. Bai C-F, Liu J-C, Zhao R, Cao W, Liu S-B, Zhang X-N, et al. Role of 5-HT2B receptors in cardiomyocyte apoptosis in noradrenaline-induced cardiomyopathy in rats. *Clin Exp Pharmacol Physiol* 2010;37:e145–e151. doi: 10.1111/j.1440-1681.2010.05388.x.

47. Lee LL, Chintalgattu V. Pericytes in the heart. Adv. Exp. Med. Biol., vol. 1122, Springer, Cham; 2019, p. 187–210. doi: 10.1007/978-3-030-11093-2_11.

48. Jaffré F, Callebert J, Sarre A, Etienne N, Nebigil CG, Launay J-M, et al. Involvement of the serotonin 5-HT2B receptor in cardiac hypertrophy linked to sympathetic stimulation: control of interleukin-6, interleukin-1beta, and tumor necrosis factor-alpha cytokine production by ventricular fibroblasts. *Circulation* 2004;110:969–974. doi: 10.1161/01.CIR.0000139856.20505.57.

49. Yang Q, Yan C, Yin C, Gong Z. Serotonin Activated Hepatic Stellate Cells Contribute to Sex Disparity in Hepatocellular Carcinoma. *CMGH* 2017;3:484–499. doi: 10.1016/j.jcmgh.2017.01.002.

50. Swonger JM, Liu JS, Ivey MJ, Tallquist MD. Genetic tools for identifying and manipulating fibroblasts in the mouse. *Differentiation* 2016;92:66–83. doi:

10.1016/j.diff.2016.05.009.

51. Vega-Benedetti AF, Saucedo CN, Zavattari P, Vanni R, Royo F, Llavero F, et al. PLAGL1 gene function during hepatoma cells proliferation. *Oncotarget* 2018;9:32775–32794. doi: 10.18632/oncotarget.25996.

52. Hassel D, Dahme T, Erdmann J, Meder B, Huge A, Stoll M, et al. Nexilin mutations destabilize cardiac Z-disks and lead to dilated cardiomyopathy. *Nat Med* 2009;15:1281–1288. doi: 10.1038/nm.2037.

53. Baardman ME, Zwier M V., Wisse LJ, Gittenberger-De Groot AC, Kerstjens-Frederikse WS, Hofstra RMW, et al. Common arterial trunk and ventricular non-compaction in Lrp2 knockout mice indicate a crucial role of LRP2 in cardiac development. *DMM Dis Model Mech* 2016;9:413–425. doi: 10.1242/dmm.022053.

54. Faul C. Cardiac actions of fibroblast growth factor 23. *Bone* 2017;100:69–79. doi: 10.1016/j.bone.2016.10.001.

55. Gould RA, Aziz H, Woods CE, Seman-Senderos MA, Sparks E, Preuss C, et al. ROBO4 variants predispose individuals to bicuspid aortic valve and thoracic aortic aneurysm. *Nat Genet* 2019;51:42–50. doi: 10.1038/s41588-018-0265-y.

56. Uhlen M, Fagerberg L, Hallstrom BM, Lindskog C, Oksvold P, Mardinoglu A, et al. Tissue-based map of the human proteome. *Science (80-)* 2015;347:1260419–1260419. doi: 10.1126/science.1260419.

57. Kaur H, Takefuji M, Ngai C, Carvalho J, Bayer J, Wietelmann A, et al. Targeted Ablation of Periostin-Expressing Activated Fibroblasts Prevents Adverse Cardiac Remodeling in Mice. *Circ Res* 2016;118:1906–1917. doi: 10.1161/CIRCRESAHA.116.308643.

58. Belmer A, Quentin E, Diaz SL, Guiard BP, Fernandez SP, Doly S, et al. Positive

regulation of raphe serotonin neurons by serotonin 2B receptors. *Neuropsychopharmacology* 2018;43:1623–1632. doi: 10.1038/s41386-018-0013-0.

59. Bonhaus DW, Flippin LA, Greenhouse RJ, Jaime S, Rocha C, Dawson M, et al. RS-127445: a selective, high affinity, orally bioavailable 5-HT 2B receptor antagonist. *Br J Pharmacol* 1999;127:1075–1082. doi: 10.1038/sj.bjp.0702632.

60. Yezzi AJ, Prince JL. An Eulerian PDE Approach for Computing Tissue Thickness. *IEEE Trans Med Imaging* 2003;22:1332–1339. doi: 10.1109/TMI.2003.817775.

61. Bersi MR, Khosravi R, Wujciak AJ, Harrison DG, Humphrey JD. Differential cell-matrix mechanoadaptations and inflammation drive regional propensities to aortic fibrosis, aneurysm or dissection in hypertension. *J R Soc Interface* 2017;14:20170327. doi: 10.1098/rsif.2017.0327.

62. Cox G, Kable E, Jones A, Fraser I, Manconi F, Gorrell MD. 3-Dimensional imaging of collagen using second harmonic generation. *J Struct Biol* 2003;141:53–62. doi: 10.1016/S1047-8477(02)00576-2.

63. Watson SR, Liu P, Peña EA, Sutton MA, Eberth JF, Lessner SM. Comparison of Aortic Collagen Fiber Angle Distribution in Mouse Models of Atherosclerosis Using Second-Harmonic Generation (SHG) Microscopy. *Microsc Microanal* 2016;22:55–62. doi: 10.1017/S1431927615015585.

64. Adams W, Mehl B, Leiser E, Wang M, Patton S, Throckmorton G, et al. Multimodal Nonlinear Optical and Thermal Imaging Platform for Label-Free Characterization of Biological Tissue. *BioRxiv* 2020:Preprint posted online August 28, 2020. doi: 10.1101/2020.04.06.023820.

65. Chen X, Nadiarynkh O, Plotnikov S, Campagnola PJ. Second harmonic generation

microscopy for quantitative analysis of collagen fibrillar structure. *Nat Protoc* 2012;7:654–669. doi: 10.1038/nprot.2012.009.

66. Schriefl AJ, Wolinski H, Regitnig P, Kohlwein SD, Holzapfel GA. An automated approach for three-dimensional quantification of fibrillar structures in optically cleared soft biological tissues. *J R Soc Interface* 2012;10:20120760–20120760. doi: 10.1098/rsif.2012.0760.

67. Lal H, Zhou J, Ahmad F, Zaka R, Vagnozzi RJ, Decaul M, et al. Glycogen synthase kinase-3α limits ischemic injury, cardiac rupture, post-myocardial infarction remodeling and death. *Circulation* 2012;125:65–75. doi: 10.1161/CIRCULATIONAHA.111.050666.

68. Jones TR, Kang IH, Wheeler DB, Lindquist RA, Papallo A, Sabatini DM, et al. CellProfiler Analyst: Data exploration and analysis software for complex image-based screens. *BMC Bioinformatics* 2008;9:482. doi: 10.1186/1471-2105-9-482.

69. Joll JE, Clark CR, Peters CS, Raddatz MA, Bersi MR, Merryman WD. Genetic ablation of serotonin receptor 2B improves aortic valve hemodynamics of Notch1 heterozygous mice in a high-cholesterol diet model. *PLoS One* 2020;15:e0238407. doi: 10.1371/journal.pone.0238407.

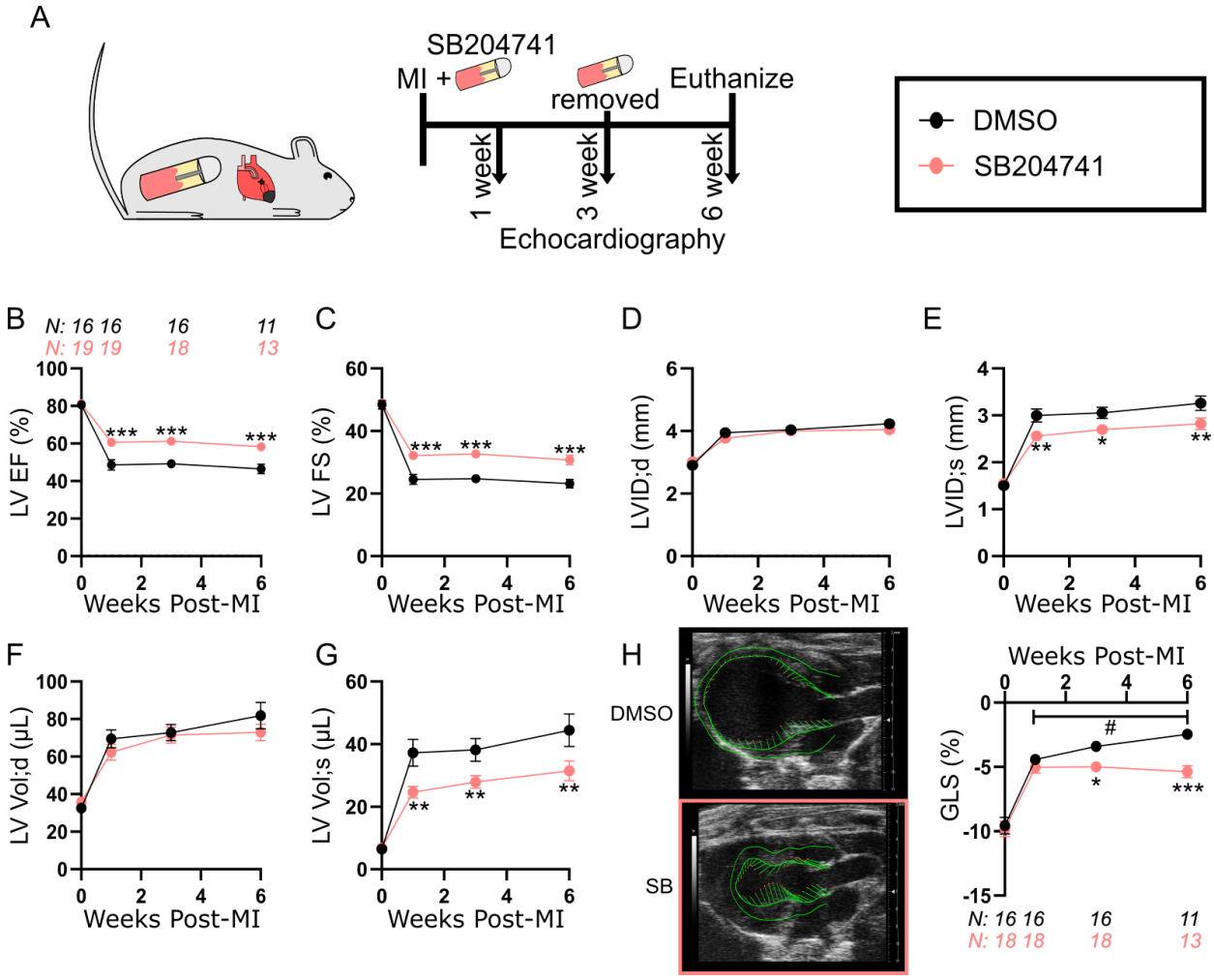

Figure 1. Antagonism of 5-HT$_{2B}$ preserves cardiac structure and function following myocardial infarction (MI) and prevents deterioration of myocardial contractile capability. **A,** Experimental approach. 12-week-old mice were subjected to MI surgery and coincidentally treated with dimethyl sulfoxide (DMSO) control or the 5-HT$_{2B}$ antagonist, SB204741 (SB). Treatment was ceased three weeks following injury, and serial echocardiography was performed at times shown. **B,** Left ventricular ejection fraction (LV EF). **C,** Left ventricular fractional shortening (LV FS). **D,E,** Left ventricular internal dimension at end-diastole (LVID;d) and end-systole (LVID;s). **F,G,** Left ventricular volume at end-diastole (LV Vol;d) and end-systole (LV Vol;s). **H,** Vector diagram showing magnitude and direction of myocardial deformation in systole and quantified global longitudinal strain (GLS). **B-H,** Mean ± SEM, *P<0.05, **P<0.01, ***P<0.001 between DMSO and SB treatments, #P<0.05 between timepoints within treatment group following 2-way ANOVA and Holm-Sidak post hoc test. Number of mice denoted in **B** applies to subsequent groups except **H** where explicitly labeled.

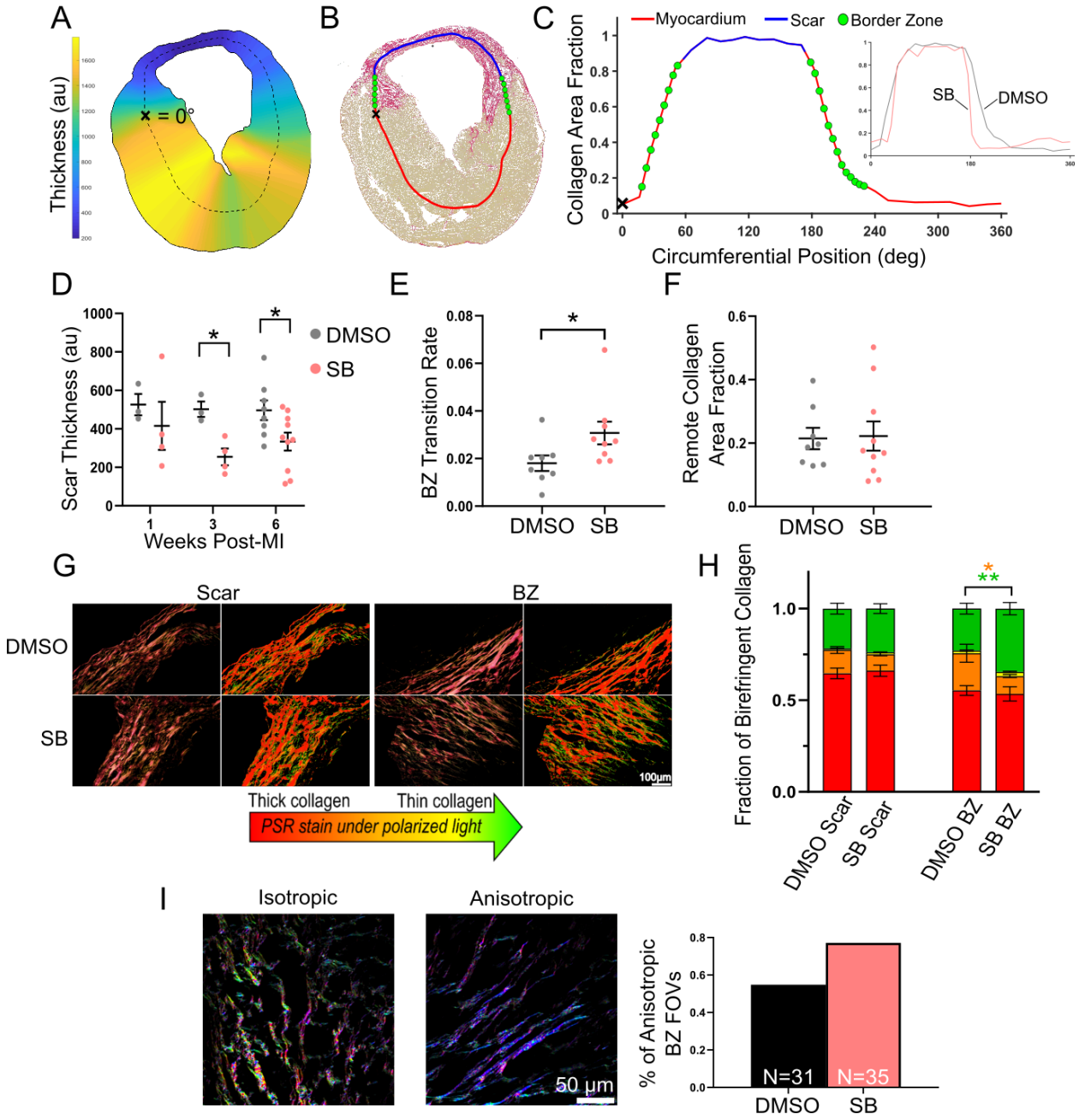

Figure 2. Diminished 5-HT$_{2B}$ signaling decreases fibrotic scar formation and border zone (BZ) expansion after myocardial infarction (MI) through alterations in collagen composition. A-C, Analytical approach of calculating tissue thickness (**A**), demarcation of scar vs. healthy myocardium (**B**), and (**C**) mathematical definition of BZ as the transition region between scar dominated (>85% collagen stained red with picrosirius red; PSR) and myocardium dominated (>85% myocardium stained yellow) with inset illustrating a representative curve from each treatment. **D,** Thickness of the formed scar is decreased with SB204741 (SB) treatment but does not thin over time (N=3-10). **E,** Decreased BZ infiltration with 5-HT$_{2B}$ antagonism as indicated by the rapid transition from scar to myocardium (N=8-10). **F,** No difference in interstitial fibrosis was observed (N=8-10). **G-H,** PSR stain imaged under polarized light in the

BZ and scar revealed an increased proportion of thinner, less mature collagen fibers in the BZ of SB-treated mice (N=9-10). **I,** Analysis of collagen fiber orientation in the BZs of DMSO- (31 FOVs across 4 mice) and SB- (35 FOVs across 5 mice) treated animals to quantify the distribution of orientations to classify as isotropic or anisotropic. All data 6 weeks post-MI except where noted in **D**. **D-F, H,** Mean ± SEM, *P<0.05, **P<0.01 (color denotes difference between corresponding color proportion in **H**) (**D,H**) 2-way ANOVA and Holm-Sidak post hoc test or (**E,F**) 2-tailed Student *t* test.

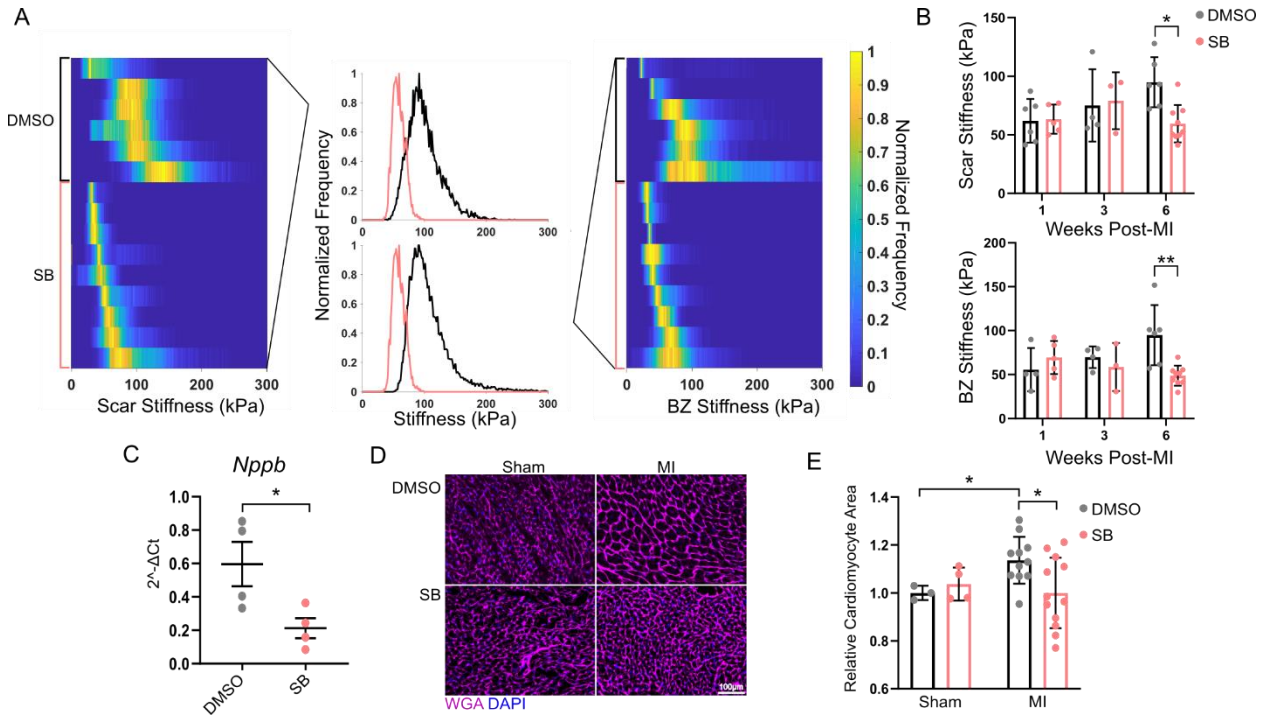

Figure 3. Tissue stiffening and concomitant increase in cardiomyocyte size are prevented with 5-HT$_{2B}$ blockade. Atomic force microscopy (AFM) was employed to analyze scar and BZ stiffness after MI. Each heart was arrested in diastole via submersion in 3M potassium chloride upon dissection. **A,** Each row illustrates the distribution of stiffness values within an individual mouse with representative histogram in the middle. **B,** Mean tissue stiffness of scar and BZ (N=3-9). **C,** qPCR analysis of *Nppb*, the gene encoding the heart failure marker natriuretic peptide B (N=4). **D-E,** Wheat germ agglutinin (WGA) staining of short-axis cardiomyocytes reveals increased cross-sectional area in control treated animals after MI compared to sham operation is prevented with 5-HT$_{2B}$ antagonism (N=3-12). **B-C, E,** Mean ± SEM, *P<0.05, **P<0.01 (**B,E**) 2-way ANOVA and Holm-Sidak post hoc test or (**C**) 2-tailed Student *t* test.

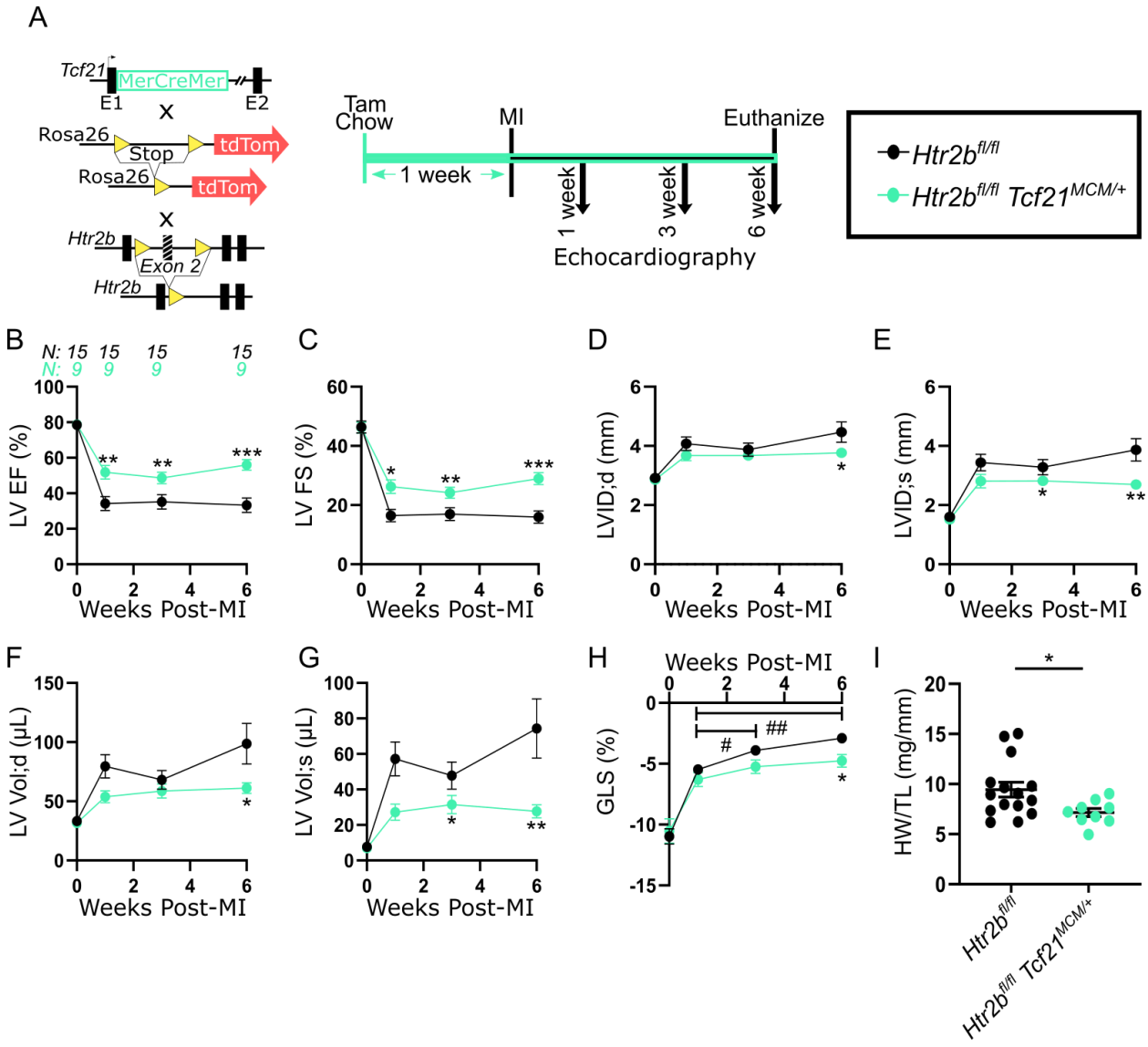

Figure 4. *Htr2b* deletion in resident cardiac fibroblasts (CFs) abates impact of myocardial infarction (MI). A, Left Schematic illustrating the *Tcf21* locus harboring a tamoxifen-inducible MerCreMer (MCM) cDNA, tdTomato reporter in the *Rosa26* locus preceded by a loxP-flanked stop codon, and a loxP-flanked *Htr2b* target allele. **Middle** Experimental timeline for 16-17-week-old mice. **Right** Key. **B,** Left ventricular ejection fraction (LV EF). **C,** Left ventricular fractional shortening (LV FS). **D,E,** Left ventricular internal dimension at end-diastole (LVID;d) and end-systole (LVID;s). **F,G,** Left ventricular volume at end-diastole (LV Vol;d) and end-systole (LV Vol;s). **H,** Global longitudinal strain (GLS). **I,** Heart weight (HW) normalized to tibia length (TL). **B-I,** Mean ± SEM, *P<0.05, **P<0.01, ***P<0.001 between *Htr2b*$^{fl/fl}$ and *Htr2b*$^{fl/fl}$*Tcf21*$^{MCM/+}$ animals, #P<0.05, ##P<0.01 between timepoints within genotype following (**B-H**) 2-way ANOVA and Holm-Sidak post hoc test or (**I**) 2-tailed Student *t* test**.** Number of mice analyzed denoted in **B** applies to all subsequent data.

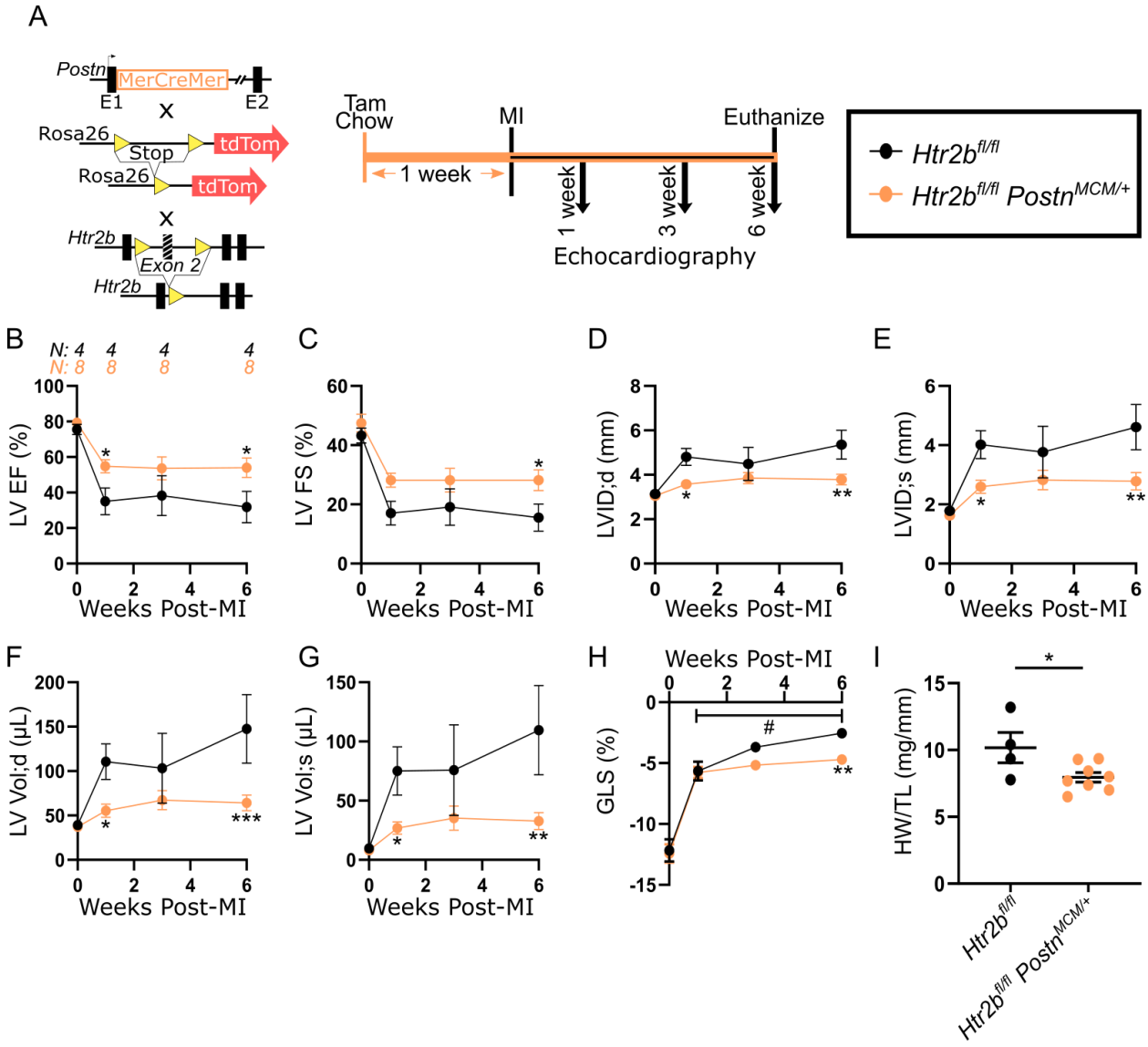

Figure 5. *Htr2b* deletion in activated myofibroblasts abates impact of myocardial infarction (MI). A, Left Schematic illustrating the *Postn* locus harboring a tamoxifen-inducible MerCreMer (MCM) cDNA, tdTomato reporter in the *Rosa26* locus preceded by a loxP-flanked stop codon, and a loxP-flanked *Htr2b* target allele. **Middle** Experimental timeline for 11-14-week-old mice. **Right** Key. **B,** left ventricular ejection fraction (LV EF). **C,** left ventricular fractional shortening (LV FS). **D,E,** Left ventricular internal dimension at end-diastole (LVID;d) and end-systole (LVID;s). **F,G,** Left ventricular volume at end-diastole (LV Vol;d) and end-systole (LV Vol;s). **H,** Global longitudinal strain (GLS). **I,** Heart weight (HW) normalized to tibia length (TL). **B-I,** Mean ± SEM, *P<0.05, **P<0.01, ***P<0.001 between *Htr2b*$^{fl/fl}$ and *Htr2b*$^{fl/fl}$*Postn*$^{MCM/+}$, #P<0.05, between timepoints within genotype following (**B-H**) 2-way ANOVA and Holm-Sidak post hoc test or (**I**) 2-tailed Student *t* test**.** Number of mice analyzed denoted in **B** applies to all subsequent data.

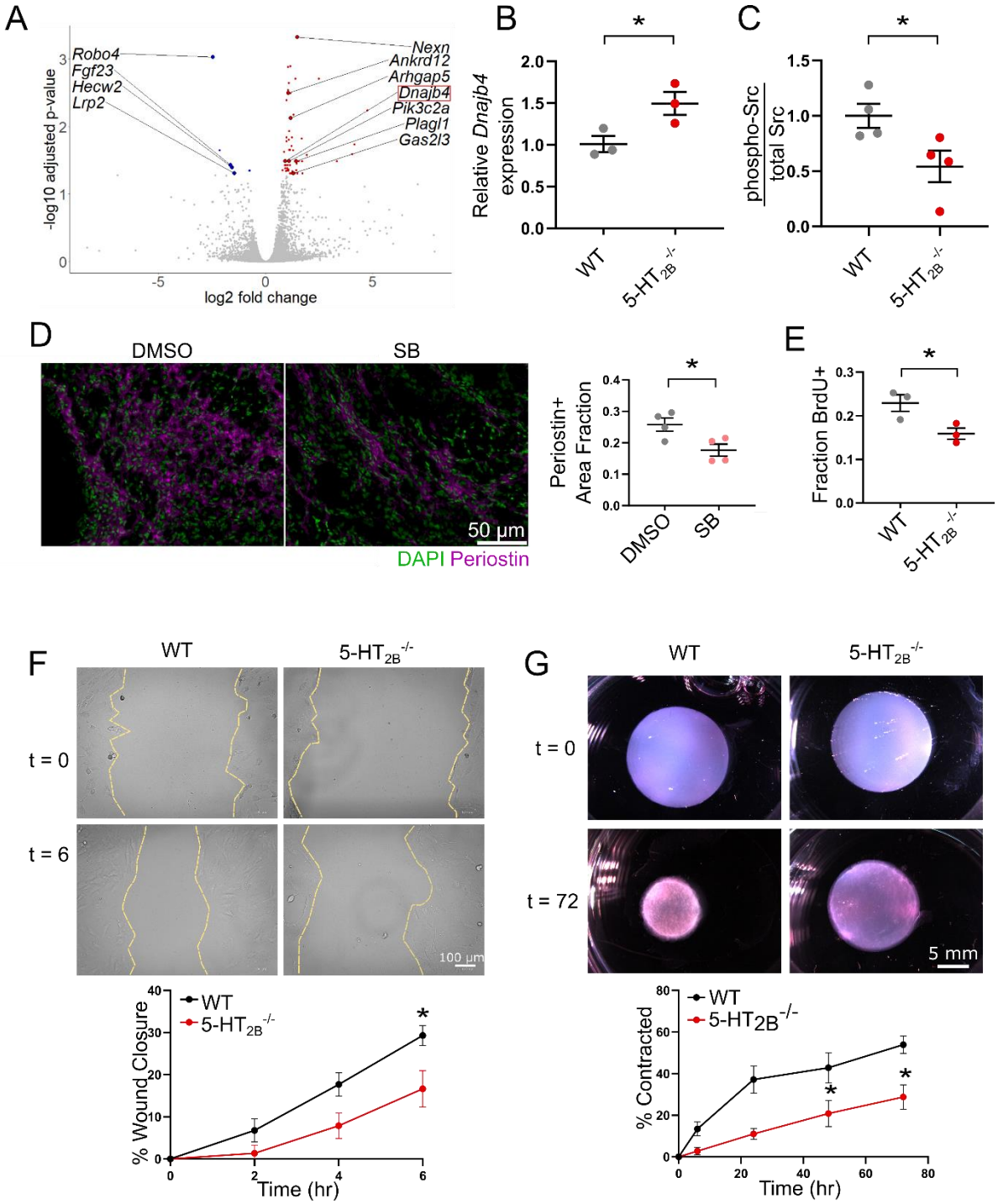

Figure 6. *Htr2b* deletion impairs proliferative and remodeling capabilities of cardiac fibroblasts (CFs). A, Volcano plot highlighting differentially regulated genes in PDGFRα+ cells isolated from *Htr2b*$^{fl/fl}$*Postn*$^{MCM/+}$ (N=4) compared to *Htr2b*$^{fl/fl}$ animals (N=2). **B,** Increased expression of *Dnajb* in 5-HT$_{2B}$-knockout CFs (N=3). **C,** Phosphorylated Src is decreased in isolated CFs lacking 5-HT$_{2B}$ (normalized to total Src and loading control α-tubulin, N=4). **D,** Periostin immunostaining reveals a decrease in myofibroblast presence in damaged tissue one

week after MI (N=4). **E,** 5-HT_{2B}-knockout CFs exhibit decreased proliferation measured by BrdU incorporation (N=3). **F,** 5-HT_{2B}-knockout CFs are less migratory than WT counterparts (N=3). **G,** Free-floating collagen gel contraction assay reveals a decrease in collagen matrix remodeling by 5-HT_{2B}-knockout CFs (N=6). **B-G,** Mean ± SEM, *P<0.05, following (**B-E**) 2-tailed Student *t* test or (**F,G**) 2-way ANOVA and Holm-Sidak post hoc test.

Figure Legends

Figure 1. Antagonism of 5-HT_{2B} preserves cardiac structure and function following myocardial infarction (MI) and prevents deterioration of myocardial contractile capability. **A,** Experimental approach. 12-week-old mice were subjected to MI surgery and coincidentally treated with dimethyl sulfoxide (DMSO) control or the 5-HT_{2B} antagonist, SB204741 (SB). Treatment was ceased three weeks following injury, and serial echocardiography was performed at times shown. **B,** Left ventricular ejection fraction (LV EF). **C,** Left ventricular fractional shortening (LV FS). **D,E,** Left ventricular internal dimension at end-diastole (LVID;d) and end-systole (LVID;s). **F,G,** Left ventricular volume at end-diastole (LV Vol;d) and end-systole (LV Vol;s). **H,** Vector diagram showing magnitude and direction of myocardial deformation in systole and quantified global longitudinal strain (GLS). **B-H,** Mean ± SEM, *P<0.05, **P<0.01, ***P<0.001 between DMSO and SB treatments, #P<0.05 between timepoints within treatment group following 2-way ANOVA and Holm-Sidak post hoc test. Number of mice denoted in **B** applies to subsequent groups except **H** where explicitly labeled.

Figure 2. Diminished 5-HT_{2B} signaling decreases fibrotic scar formation and border zone (BZ) expansion after myocardial infarction (MI) through alterations in collagen composition. A-C, Analytical approach of calculating tissue thickness (**A**), demarcation of scar vs. healthy myocardium (**B**), and (**C**) mathematical definition of BZ as the transition region between scar dominated (>85% collagen stained red with picrosirius red; PSR) and myocardium dominated (>85% myocardium stained yellow) with inset illustrating a representative curve from each treatment. **D,** Thickness of the formed scar is decreased with SB204741 (SB) treatment but does not thin over time (N=3-10). **E,** Decreased BZ infiltration with 5-HT_{2B} antagonism as indicated by the rapid transition from scar to myocardium (N=8-10). **F,** No difference in

interstitial fibrosis was observed (N=8-10). **G-H,** PSR stain imaged under polarized light in the BZ and scar revealed an increased proportion of thinner, less mature collagen fibers in the BZ of SB-treated mice (N=9-10). **I,** Analysis of collagen fiber orientation in the BZs of DMSO- (31 FOVs across 4 mice) and SB- (35 FOVs across 5 mice) treated animals to quantify the distribution of orientations to classify as isotropic or anisotropic. All data 6 weeks post-MI except where noted in **D**. **D-F, H,** Mean ± SEM, *P<0.05, **P<0.01 (color denotes difference between corresponding color proportion in **H**) (**D,H**) 2-way ANOVA and Holm-Sidak post hoc test or (**E,F**) 2-tailed Student *t* test.

Figure 3. Tissue stiffening and concomitant increase in cardiomyocyte size are prevented with 5-HT_{2B} blockade. Atomic force microscopy (AFM) was employed to analyze scar and BZ stiffness after MI. Each heart was arrested in diastole via submersion in 3M potassium chloride upon dissection. **A,** Each row illustrates the distribution of stiffness values within an individual mouse with representative histogram in the middle. **B,** Mean tissue stiffness of scar and BZ (N=3-9). **C,** qPCR analysis of *Nppb*, the gene encoding the heart failure marker natriuretic peptide B (N=4). **D-E,** Wheat germ agglutinin (WGA) staining of short-axis cardiomyocytes reveals increased cross-sectional area in control treated animals after MI compared to sham operation is prevented with 5-HT_{2B} antagonism (N=3-12). **B-C, E,** Mean ± SEM, *P<0.05, **P<0.01 (**B,E**) 2-way ANOVA and Holm-Sidak post hoc test or (**C**) 2-tailed Student *t* test.

Figure 4. *Htr2b* deletion in resident cardiac fibroblasts (CFs) abates impact of myocardial infarction (MI). A, Left Schematic illustrating the *Tcf21* locus harboring a tamoxifen-inducible MerCreMer (MCM) cDNA, tdTomato reporter in the *Rosa26* locus preceded by a loxP-flanked

stop codon, and a loxP-flanked *Htr2b* target allele. **Middle** Experimental timeline for 16-17-week-old mice. **Right** Key. **B,** Left ventricular ejection fraction (LV EF). **C,** Left ventricular fractional shortening (LV FS). **D,E,** Left ventricular internal dimension at end-diastole (LVID;d) and end-systole (LVID;s). **F,G,** Left ventricular volume at end-diastole (LV Vol;d) and end-systole (LV Vol;s). **H,** Global longitudinal strain (GLS). **I,** Heart weight (HW) normalized to tibia length (TL). **B-I,** Mean ± SEM, *P<0.05, **P<0.01, ***P<0.001 between $Htr2b^{fl/fl}$ and $Htr2b^{fl/fl}Tcf21^{MCM/+}$ animals, #P<0.05, ##P<0.01 between timepoints within genotype following (**B-H**) 2-way ANOVA and Holm-Sidak post hoc test or (**I**) 2-tailed Student *t* test**.** Number of mice analyzed denoted in **B** applies to all subsequent data.

Figure 5. *Htr2b* deletion in activated myofibroblasts abates impact of myocardial infarction (MI). A, Left Schematic illustrating the *Postn* locus harboring a tamoxifen-inducible MerCreMer (MCM) cDNA, tdTomato reporter in the *Rosa26* locus preceded by a loxP-flanked stop codon, and a loxP-flanked *Htr2b* target allele. **Middle** Experimental timeline for 11-14-week-old mice. **Right** Key. **B,** left ventricular ejection fraction (LV EF). **C,** left ventricular fractional shortening (LV FS). **D,E,** Left ventricular internal dimension at end-diastole (LVID;d) and end-systole (LVID;s). **F,G,** Left ventricular volume at end-diastole (LV Vol;d) and end-systole (LV Vol;s). **H,** Global longitudinal strain (GLS). **I,** Heart weight (HW) normalized to tibia length (TL). **B-I,** Mean ± SEM, *P<0.05, **P<0.01, ***P<0.001 between $Htr2b^{fl/fl}$ and $Htr2b^{fl/fl}Postn^{MCM/+}$, #P<0.05, between timepoints within genotype following (**B-H**) 2-way ANOVA and Holm-Sidak post hoc test or (**I**) 2-tailed Student *t* test**.** Number of mice analyzed denoted in **B** applies to all subsequent data.

Figure 6. *Htr2b* deletion impairs proliferative and remodeling capabilities of cardiac fibroblasts (CFs). A, Volcano plot highlighting differentially regulated genes in PDGFRα+ cells isolated from $Htr2b^{fl/fl}Postn^{MCM/+}$ (N=4) compared to $Htr2b^{fl/fl}$ animals (N=2). **B,** Increased expression of *Dnajb* in 5-HT_{2B}-knockout CFs (N=3). **C,** Phosphorylated Src is decreased in isolated CFs lacking 5-HT_{2B} (normalized to total Src and loading control α-tubulin, N=4). **D,** Periostin immunostaining reveals a decrease in myofibroblast presence in damaged tissue one week after MI (N=4). **E,** 5-HT_{2B}-knockout CFs exhibit decreased proliferation measured by BrdU incorporation (N=3). **F,** 5-HT_{2B}-knockout CFs are less migratory than WT counterparts (N=3). **G,** Free-floating collagen gel contraction assay reveals a decrease in collagen matrix remodeling by 5-HT_{2B}-knockout CFs (N=6). **B-G,** Mean ± SEM, *P<0.05, following (**B-E**) 2-tailed Student *t* test or (**F,G**) 2-way ANOVA and Holm-Sidak post hoc test.

Supplemental Materials

Expanded Materials & Methods

Mice

Mice used in this study were wild type (WT) C57BL/6 (Jackson Laboratory, Stock No. 000664), floxed *Htr2b* mice (*Htr2b*$^{fl/fl}$) [58], *Postn*^{MCM} provided by Dr. Jeffery Molkentin (Cincinnati Children's Hospital Medical Center)[6], *Tcf21*^{MCM} provided by Dr. Michelle Tallquist (University of Hawaii)[31], *Htr2b* mutant mice[29], WT mice expressing the CD45.1 allele for bone marrow transplantation studies (Jackson Laboratory, Stock No. 002014), and *Rosa26*-stop-tdTomato reporter mice (Jackson Laboratory, Stock No. 007914).

Cell-specific 5-HT_{2B} knockout animals were generated by mating *Htr2b*$^{fl/fl}$*;R26*tdTomato$^{+/+}$ females with either *Htr2b*$^{fl/fl}$*Postn*$^{MCM/+}$ *or Htr2b*$^{fl/fl}$*Tcf21*$^{MCM/+}$ males to ensure progeny had either zero (littermate control) or one (experimental) copy of MCM cDNA, 1 copy of the reporter gene, and were homozygous *Htr2b*$^{fl/fl}$.

Animal Studies

Myocardial infarction (MI) was induced in 11- to 17-week-old mice by permanent coronary artery ligation, as previously described.[24–26] Briefly, mice were anesthetized with 2% isoflurane inhalation. A small incision was made over the left chest and dissection and retraction of the pectoral major and minor muscle was performed. A small whole was punctured in the fourth intercostal space and gently held open with a mosquito clamp. Using gentle pressure

superior and inferior to the heart, the heart was popped out of the chest. A 6-0 silk suture was used to ligate the left main descending coronary artery approximately 2 mm from its origin. The heart was immediately placed back into the chest cavity, air was manually evacuated, the muscle was replaced, and the skin sutured. For antagonist studies, male mice (except for the specific study done in females) were administered 1 mg/kg/day of either the 5-HT_{2B} antagonist SB204741 (SB; Tocris, Cat. No. 1372) or RS127445 hydrochloride (RS; Tocris, Cat. No. 2993) – both dissolved in a 50:50 mixture of PEG400 (Fisher Scientific, P167-1) and dimethyl sulfoxide (DMSO; Sigma D8418). Control mice were administered 50:50 PEG400:DMSO. SB was administered subcutaneously via micro-osmotic pumps (Alzet Corp, 1004). RS was administered through twice-daily intraperitoneal injections of 0.5 mg/kg separated by 7-9 hours due to the limited half-life of the compound *in vivo*.[59] *Htr2b*$^{fl/fl}$*Tcf21*$^{MCM/+}$, *Htr2b*$^{fl/fl}$*Postn*$^{MCM/+}$, and *Htr2b*$^{fl/fl}$ control mice (including male and females as indicated in Supplemental Figures 10-11) were administered tamoxifen chow (Envigo, TD. 130860) exclusively one week prior to surgery and maintained throughout the remainder of the study. The perioperative phase was defined as the 4-6 hours following surgery as mice were monitored until ambulatory again. Mortality in this window was attributed to surgical errors and no data from animals in this window was included.

For bone marrow transplantation studies, 6- to 8-week-old male mice carrying the CD45.1 hematopoietic marker were given a split 12 Gy dose of radiation from a Cs^{137} source. Twenty-four hours following, 1 – 2.5x10^6 bone marrow cells isolated from age- and sex-matched cogenic WT or *Htr2b*$^{-/-}$ donors (carrying the CD45.2 allele) were transplanted via retro-orbital injection.[20] Six weeks were given for reconstitution, then permanent occlusion MI was performed. Transplant efficiency was confirmed by flow cytometry of isolated bone marrow by

observing the engraftment of donor cells expressing the CD45.2 allele with concomitant absence of the native CD45.1 allele.

At the end of each study, mice were euthanized through CO_2 inhalation in accordance with Vanderbilt University Medical Center's Division of Animal Care guidelines.

Echocardiography

Blinded echocardiographic measurements were taken from short-axis cardiac M-mode images captured at mid-papillary level of non-anesthetized mice on a Vevo2100 small-animal ultrasound system (VisualSonics). A minimum of 9 independent measurements of ventricle diameters were used to calculate metrics of cardiac structure and function for each mouse at each time point [EF = (LV Vol;d – LV Vol;s)/LV Vol;d; FS = (LVID;d – LVID;s)/LVID;s]. Global longitudinal strain (GLS) measurements were acquired using the VevoStrain software package to measure long-axis B-mode images (VisualSonics) at the initiation of contraction. Two independent images were analyzed for each mouse at each time point. Measurements were taken prior to surgery (Day 0), as well as one, three, and six weeks post-surgery. Exclusion criteria were employed for animals without a 15% decrease or more than an 85% decrease in ejection fraction at day seven compared to day zero to ensure that surgery was successful.

Histology

Upon euthanasia, hearts were perfused with PBS-/-, excised, and submerged in 3 M potassium chloride to arrest hearts in diastole. Hearts were then bisected along the transverse

plane just above where the suture was tied to occlude the left main descending coronary artery, embedded in OCT media (Fisher Scientific, 23-730-571), and snap frozen. Frozen tissue was cryosectioned at 7 µm, mounted onto glass slides, then stored at -20°C. Picrosirius red staining was used to identify ECM (red) and cytoplasm (yellow). Prior to staining, slides were brought to room temperature, OCT was removed via PBS-/- wash, and sections were fixed for one hour in Bouin's solution (Sigma-Aldrich, HT10132) at 55°C. Slides were stained in picrosirius red (Electron Microscopy Sciences, 26357) for one hour at room temperature, dehydrated in ethanol, and cleared in xylenes. Images were analyzed using a semiautomated image-processing pipeline that was developed based on local ventricular thickness measurements and color segmentation.[60,61] This process extracted regional area fractions of myocardium and fibrosis as well as local thickness values used to quantify tissue properties. The border zone (BZ) was defined by the change in collagen area fraction per circumferential degree in the transition region lying between tissues comprised of 85% collagen (scar) to 15% collagen (uninjured myocardium). Picrosirius red-stained sections were imaged under polarized light to study collagen fiber thickness distributions and analyzed using a color segmentation algorithm as previously described.[61]

Infarct area was determined as previously described, one millimeter thick sections of infarcted LV were obtained 24 hours after infarct. Tissue was incubated in 2% 2,3,5-Triphenyltetrazolium chloride (TTC) in PBS for 30 minutes at 37°C to differentiate between infarcted and viable tissue. ImageJ was used to quantify total and infarcted LV area.

Second Harmonic Generation

SHG produces images with a diffraction-limited resolution (<300 nm), is intrinsic to specific structures allowing for quantification of collagen without staining or background noise, and can be used to classify the anisotropic properties of collagen fibers.[62,63] Second harmonic generation (SHG) images were acquired using home built multimodal imaging platform equipped with a photomultiplier tube (GaAsP Amplified PMT, Thorlabs, USA) on the epi-detection port.[64] Each image was integrated for 7 microseconds/pixel and recorded using a 20x water immersion objective (Olympus XLUMPLFLN, 1.0NA) with a high spatial sampling density (401 nm/pixel) covering 1024x1024 pixels per image. SHG signals were generated using 798 nm picosecond laser operates with a pulse repetition rate of 80MHz (power ~30mW on the sample) and collected at using 400/±40nm filter (Semrock, Brattleboro, VT, USA). Scanning and detection for imaging is controlled through ThorImageLS version 2.1 (Thorlabs Imaging Research, Sterling, VA, USA).

The OrientationJ plugin was used in ImageJ (NIH) to obtain the distribution of fiber angles from each image.[65] Each distribution was smoothed using a centered moving average with a five degree window, followed by calculation of the cumulative distribution function (CDF),

$$F(\Phi) = \sum_{\Phi_i=-89.5°}^{x} I(\Phi_i)$$

where I(Φ) is the amplitude of the distribution at angle Φ. The CDF of an isotropic distribution is a straight line. Therefore, we a fit a first-degree polynomial to the distribution and calculated the correlation coefficient (R^2) as a goodness of fit. Supplemental Figure 5 shows a range of obtained R^2 value from accompanying SHG images and fiber angle distributions. If the R^2 was above a threshold of 0.98 (below which dominant orientations in fiber orientation started to

peak), the distribution was considered isotropic, otherwise, the distribution was considered anisotropic.[66]

Atomic Force Microscopy (AFM)

Tissue sections which had been arrested in diastole using 3 M potassium chloride upon dissection were brought to room temperature and cleared of OCT in PBS-/-. A Biocatalyst AFM (Bruker, CA) was used to measure tissue topology and stiffness. The AFM was operated in peak force quantitative nanomechanical mapping scanning mode (Peak Force QNM) using probes constituted of blunted pyramidal tips designed for biological samples (MLCT-Bio). The system was calibrated to obtain the spring constant and deflection sensitivity of each probe then confirmed on standard polyacrylamide gels of known stiffness (2, 20, and 40 kPa). Measurements were made in PBS for the scar, BZ, and remote myocardium by scanning three to six regions of 36 – 100 μm^2 each. Mean elastic modulus was calculated for each scan, then averaged for each mouse.

Adult Cardiomyocyte Isolation

Adult cardiomyocytes were isolated as previously described.[67] Mice were treated with 50 U heparin and anesthetized by intraperitoneal Avertin injection. The heart was excised and cannulated for retrograde perfusion in a Langendorff apparatus at a constant flow rate of 3 mL/min at 37°C. The heart was perfused for 5 minutes with isolation buffer [120 mmol/L NaCl, 5.4 mmol/" KCl, 1.2 mmol/L $MgSO_4$, 1.2 mmol/L NaH_2PO_4, 5.6 mmol/L glucose, 5 mmol/L

$NaHCO_3$, 10 mmol/L HEPES, 50 µmol/L $CaCl_2$, 10 mmol/L 2,3-butanedione monoxime, and 5 mmol/L taurine] and subsequently digested for 13 minutes with collagenase II (1.5 mg/mL, Worthington Biochemical) in isolation buffer. Following digestion, hearts were removed and cardiomyocytes suspended in isolation buffer. Serial centrifugation and resuspension were performed 4 times to reintroduce Ca^{2+} in a stepwise manner from 50 µmol/L to 1.0 mmol/L. Total RNA was extracted using the RNeasy Mini kit (Qiagen, 74104). cDNA synthesis was performed using iScript cDNA synthesis kit (Bio-Rad, 170-8891). qPCR was performed using TaqMan Gene Expression Master Mix (Applied Biosystems, 4369016) and the TaqMan gene expression assays (Eukaryotic 18S rRNA Endogenous Control Cat#4319413E and Htr2b Cat#4331182).

WGA and Immunofluorescent Staining

For wheat germ agglutinin (WGA) analysis, tissue sections which had been arrested in diastole upon dissection were brought to room temperature and OCT was removed via HBSS wash. The tissue was fixed in 4% paraformaldehyde for 15 min at 37°C then stained in 50 µg/mL WGA (Invitrogen, Cat# W11262) for 30 minutes at room temperature. Three, 20x images of short-axis cardiomyocytes were taken in the uninjured myocardium. Cardiomyocyte area was calculated using a custom pipeline in CellProfiler.[68] A minimum of 580 cells were quantified per animal.

For periostin area fraction analysis, 7 µm tissue sections were brought to room temperature and OCT was removed with a PBS-/- wash. After fixation/permeabilization (4% paraformaldehyde and 0.1% Triton X-100), cells were blocked in 5% bovine serum albumin in

PBS-/- for one hour. Cells were stained with primary antibody against periostin (1:50; abcam, ab215199) overnight. Tissue was rinsed, stained with Alexa Fluor 647 secondary antibody (1:200; Invitrogen, A-21245) for one hour, then mounted in ProLong Gold with DAPI (Thermo-Fisher Scientific, P36941). Three fields of view in the infarcted area were taken per sample on an Olympus BX53 microscope equipped with a high resolution Qimaging Retiga 3000 camera at 20x magnification. Consistent imaging parameters were used, and no-stain and secondary-only stained controls can be seen in Supplemental Figure 18. Quantitative image analysis was performed to extract area fractions using a previously described, custom MATLAB script.[61,69]

Flow Cytometry and Fluorescence-activated Cell Sorting (FACS)

Engraftment of bone marrow transplantation was tested using flow cytometry. Peripheral blood was obtained via cardiac puncture into a K-EDTA-loaded syringe. Red blood cells were immediately lysed (BioLegend, 420301), and the solution was centrifuged, resuspended in FACS buffer (PBS + 3% FBS), and filtered. Cells were labeled with DAPI (1:100,000; Thermo-Fisher Scientific) to identify dead cells then stained with conjugated antibodies: Ter-119 (1:100; violetFluor™ 450 clone; Tonbo Biosciences), CD45.1 (1:100; PE clone A20; BD Biosciences), and CD45.2 (1:100; PErCP-Cy5.5 clone 104; Tonbo Biosciences). Cells were analyzed using a BD LSRFortessa. The percentage of CD45.2+ donor cells was used as the metric of engraftment.

Isolation of CD31+ and CD45+ cells for qPCR and CFs for RNA sequencing was performed via FACS. Hearts were excised, and the atria and greater vessels were removed. The heart was cut transversely at the suture to isolate scar tissue which was then finely minced. Hearts were placed in > 175 units/mL collagenase type 2 (Worthington Biochemical, LS004202)

at 37°C for 30 minutes, triturated, and replaced at 37°C for 15 minutes. Tissue was filtered through a 70 µm cell strainer, centrifuged at 350g at 4°C, and resuspended in 1x red blood cell lysis buffer for 10 minutes at room temperature. Tissue was filtered through a 40 µm cell strainer, centrifuged, and resuspended in FACS buffer with Fc block (1 µl/ 1 x 10^6 cells; BD Biosciences 553141) for 10 minutes on ice. Cells were then stained at 4°C for 30 minutes with DAPI (1:500,000), Ter-119 (1:400; violetFluor™ 450 clone; Tonbo Biosciences), CD45.2 (1:100; PErCP-Cy5.5 clone 104; Tonbo Biosciences), CD31 (1:100; PE-Cy7; eBioscience) and CD140a to identify CFs (PDGF Receptor α; 1:400; APC clone APA5; Invitrogen). Cells were analyzed using a BD LSRFortessa. DAPI-Ter119-PDGFRα+ cells were collected for RNA sequencing.

RNA Sequencing

Cells were isolated via FACS from infarcted tissue one week after MI from *Htr2b*$^{fl/fl}$*Postn*$^{MCM/+}$ (N=4) and *Htr2b*$^{fl/fl}$ (N=2) mice. Cells were homogenized in TRIzol reagent then RNA was isolated using the Zymo Direct-zol RNA Microprep kit (Zymo, R2060). RNA integrity was measured with an Agilent Bioanalyzer prior to library preparations (Supplemental Figure 12).

The Vanderbilt Technologies for Advanced Genomics (VANTAGE) center performed library preparation, sequencing, and read alignment. Briefly, cDNA libraries were generated using NEBNext Ultra II Directional RNA Library Prep kits (New England BioLabs, E7760) then sequenced on an Illumina NovaSeq 6000 to an average depth of 84.7± 3.5 M reads per sample using 150bp paired-end chemistry. Sequencing quality was assessed using FastQC v. 1.0.0. Reads were aligned to mouse genome mm10 v. GRCm38.99 using a STAR based aligner and

gene counts were quantified, both using Illumina's DRAGEN RNA Pipeline v. 3.6.3. Gene count data was imported to R using tximport for further analysis.

Differential gene expression analysis was performed using the R package DEseq2 using Cook's outliers to filter low gene counts (mean count < 7) and false discovery rate < 0.05. All analysis was limited to protein coding genes. We did not use a fold-change cutoff when defining significantly different genes, but only 2 of the 63 differentially expressed genes had a fold change of less than 50% (*H2-Q6* and *Rps3a1*). GO and KEGG over-representation analysis was performed on all differentially expressed, protein-coding genes with the R package clusterProfiler using the respective *enrich* function with default parameters. Gene sets were considered over-represented if $p_{adj} < 0.05$. Visualizations were generated using a combination of enrichplot and ggplot2 in R. RNA sequencing data generated in this manuscript have been deposited in GEO (Gene Expression Ominbus) of NCBI under accession code GSE157520.

qPCR

A cohort of animals was set aside exclusively for qPCR and dissected under RNase-free conditions and immediately snap frozen. Samples were subsequently thawed, and scar tissue was isolated and homogenized using a bead beater and lysis matrix tubes (MP Biomedicals, 116923050). RNA was isolated using the RNeasy Mini Kit (Qiagen, 74104) and cDNA was synthesized using the Superscript IV system (Invitrogen, 18091050). Real time qPCR was performed using SYBR Green PCR Supermix (Bio-Rad, 1708882), the primers listed in Supplemental Table 3, and a Bio-Rad CFX96 C100 thermocycler. *Gapdh* and *Hprt1* were used as housekeeping genes. Statistical analysis was run on delta Ct values.

Cell isolation and Culture

WT and *Htr2b*$^{-/-}$ animals were mated with mice harboring the *Immorto* gene to allow for serial cell-culture of littermate WT and *Htr2b*$^{-/-}$ knockout cell lines. Cardiac fibroblasts (CFs) were isolated from eight-week-old mice. Hearts were excised, minced, and digested in > 175 units/mL collagenase type 2 (Worthington Biochemical, LS004202) at 37° with mixing for 45 minutes. Digested tissue was centrifuged, filtered through a 40 μm filter, and cells were plated on gelatin-coated dishes. Cells were cultured at 33°C in DMEM supplemented with 10% FBS, 1% penicillin/streptomycin, and 10 μg/mL recombinant murine interferon γ to induce activation of the simian virus 40 T antigen. Prior to experiments (overnight), cells were incubated at 37°C in the same media lacking interferon γ (complete media) to deactivate the T antigen that confers immortalization.

Western Blot

CFs were cultured in DMEM (without interferon γ) and low serum (0.1%) for 3 hours. Cells were then lysed with RIPA buffer and frozen at -80°C. Protein lysate was linearized via β-mercaptoethanol and heating for five minutes at 100°C. Electrophoresis was conducted in a 10% polyacrylamide gel, and proteins were transferred to nitrocellulose membrane (LI-COR, 926) and blocked with Odyssey Blocking Buffer (LI-COR, 927). Membranes were incubated serially overnight at 4°C with primary antibody against phosphorylated Src (1:500; Cell Signaling Technologies, 2101S), total Src (1:1,000; Cell Signaling Technologies, 2110S), and α-tubulin

(1:1000; Vanderbilt MCBR Core) followed by secondary antibodies conjugated to fluorescent tags (1:15,000; IRDye 800CW and IRDye 680RD, LI-COR, 926-32211 and 926-68070). Membranes were scanned on a LI-COR Odyssey fluorescent scanner, quantified with densitometry (Image Studio Lite), and phospho-Src normalized to total Src and α-tubulin.

Collagen Gel Contraction

CFs suspended in complete media were used to create a 50:50 mixture with a bovine collagen solution (Advanced Biomatrix, 5005) for a final collagen concentration of 1.5 mg/mL collagen and 200,000 cells/mL. 250 µL of solution was pipetted unto a Teflon ring within a suspension cell culture plate. Following 1.5 hours of polymerization, complete media was added, and the collagen gel was released from both the Teflon mold and bottom of the plate. Gels were imaged immediately after release as well as six, 24, 48, and 72 hours following. Gel area was measured at each time point using ImageJ (NIH) and normalized to original gel area.

Cell Proliferation and Migration Assay

To measure cell proliferation, 5,000 cells/cm^2 were plated in a six-well dish for 24 hours. Cells were labeled with 5-bromo-2-deoxyuridine (BrdU; 1:1,000; GE Healthcare, RPN201) for two hours then fixed in 4% paraformaldehyde for 20 minutes at room temperature. Cell membranes were permeabilized using 0.05% Triton X-100 (Sigma-Aldrich, T8787) for 10 minutes followed by nuclear permeabilization using 2N HCl for 20 minutes. Cells were stained with anti-BrdU antibody (1:200; Santa Cruz Biotechnology, SC-32323) overnight. Coverslips

were mounted in ProLong Gold with DAPI (Thermo-Fisher Scientific, P36941) in order to count total and BrdU+ nuclei.

Cell migration was quantified by first plating 15,000 cells/cm^2 in a 12-well dish and allowing them to adhere overnight and form a confluent monolayer. A 200 uL micropipette tip was dulled on the lid of the dish then used to create an artificial wound by dragging the tip down the center of the well. The center of the well was marked on the bottom of the dish to ensure imaging of a consistent area. Images were acquired at time of injury, and two, four, and six hours after injury. The cell front was measured and % closure was calculated over time using the ImageJ (NIH) software.

For both assays, three independent cell lines were used for each genotype and performed in triplicates.

Recombination Confirmation

To test recombination efficiency, *Htr2b*$^{fl/fl}$ *Tcf21*$^{MCM/+}$ animals harboring the Rosa26-stop-tdTomato reporter were fed tamoxifen chow for two weeks. Hearts were digested as previously described for flow cytometry, and viable, single, tdTomato-expressing cells were collected. Genetic DNA was isolated using the DNeasy Blood and Tissue Kit (Qiagen, 69504). PCR was conducted to identify three targets: floxed allele before recombination with reverse primer sitting within DNA that is excised upon recombination, recombined allele with primers outside the targeted exon which will only amplify under our cycling conditions if recombination has occurred, and the WT, non-floxed allele as a positive control.

Statistical Analysis

Statistical analysis was performed using SigmaPlot version 11. Shapiro-Wilk test was used to test for data normality. Subsequent statistical analyses used either a 2-way ANOVA with Holm-Sidak post hoc or a Kruskal-Wallis rank-sum test with Conover-Iman post hoc test for nonparametric data. A two-tailed Student *t* test was used for comparisons of two normally distributed groups. Applicable tests and significance are labeled in figure captions with $P<0.05$ as the cutoff for data to be considered significantly different.

Supplemental Figures

Supplemental Figure 12: Mice lacking 5-HT_{2B} in bone marrow-derived cells do not exhibit an improved phenotype after myocardial infarction (MI) compared to mice with wild-type (WT) bone marrow.

Supplemental Figure 13: Verification of Cre activation in *Htr2b*$^{fl/fl}$*Tcf21*$^{MCM/+}$ animals.

Supplemental Figure 14: Survival of resident fibroblast and myofibroblast knockout animals.

Supplemental Figure 15: Verification of Cre activation in *Htr2b*$^{fl/fl}$*Postn*$^{MCM/+}$ animals.

Supplemental Figure 16: PDGFRα+ cell isolation and RNA-sequencing quality control

Supplemental Figure 17: Raw western blot images for pSrc quantification.

Supplemental Figure 18: Controls for periostin immunostaining.

Supplemental Table 1. Heart rate ± SEM.

Supplemental Table 2. Significantly altered GO terms from RNA sequencing (BP = biological process, CC = cellular component).

Supplemental Table 3. Primer sets used for qPCR.

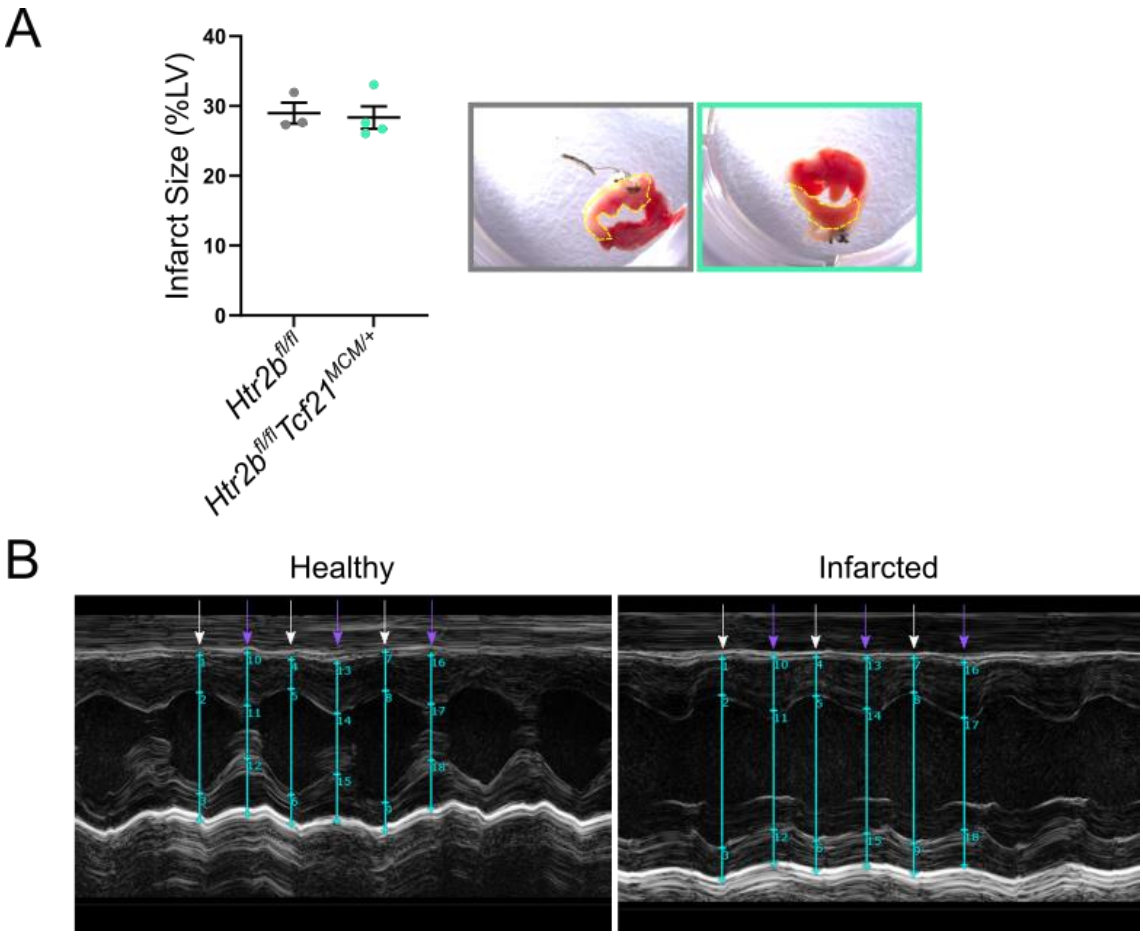

Supplemental Figure 1. Quantification of infarcted left ventricle area and representative echocardiographic images. A, TTC stain was used to demarcate infarcted tissue 24 hours after injury and area was quantified in ImageJ to confirm consistent infarct size between groups. **B,** Representative M-mode echocardiographic images from healthy and infarcted mice. Three diastolic (white arrows) and three systolic (purple arrows) cycles were analyzed for each image, and three images for each time point were analyzed per mouse.

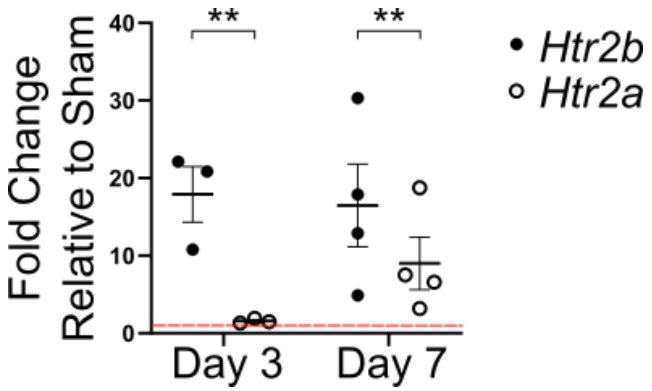

Supplemental Figure 2. *Htr2b* expression increases early and is sustained following myocardial infarction (MI). The gene encoding 5-HT_{2B}, but not 5-HT_{2A} is significantly upregulated compared to sham operation (red dashed line) three days after MI surgery and remains significantly upregulated seven days after MI (N=3-4). Mean ± SEM, **P<0.01, via 2-tailed Student *t* test**.**

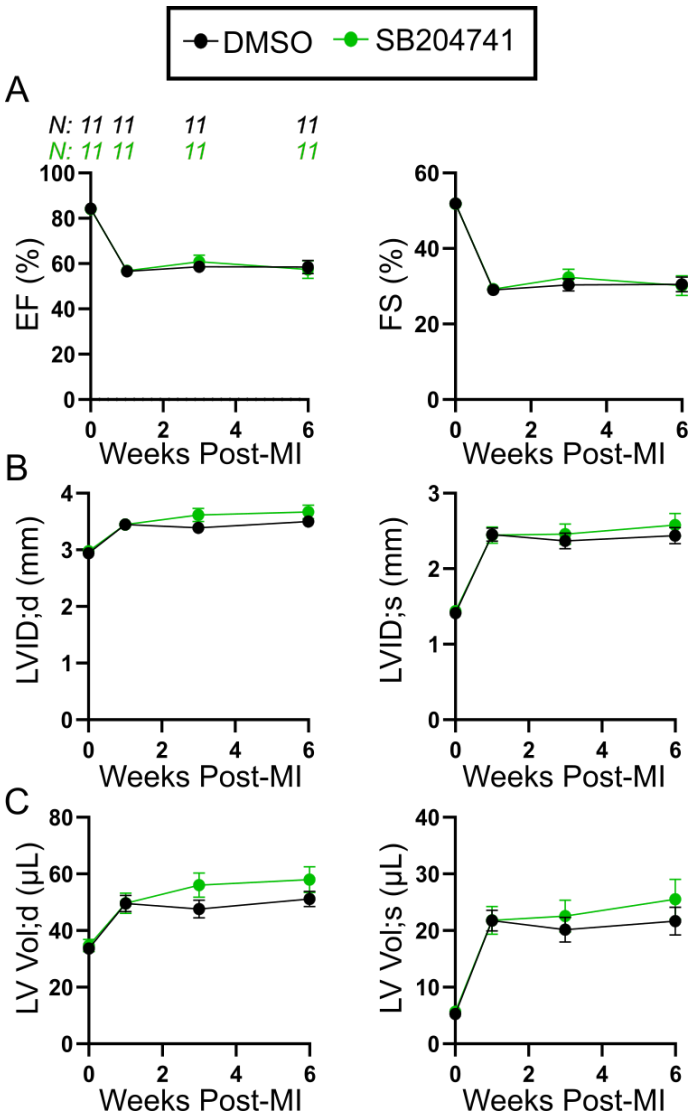

Supplemental Figure 3. 5-HT$_{2B}$ antagonism does not alter cardiac structure or function following myocardial infarction (MI) in females. 12-week-old female mice underwent MI surgery. **A,** No difference in ejection fraction (EF) or fractional shortening (FS) was observed between dimethyl sulfoxide (DMSO) control and SB204741 (SB) treated female mice. **B,** Left ventricular inner dimension (LVID) at both end-diastole and end-systole were similar between the two treatments. **C,** Left ventricular volume (LV Vol) at both end-diastole and end-systole were similar between the two treatments.

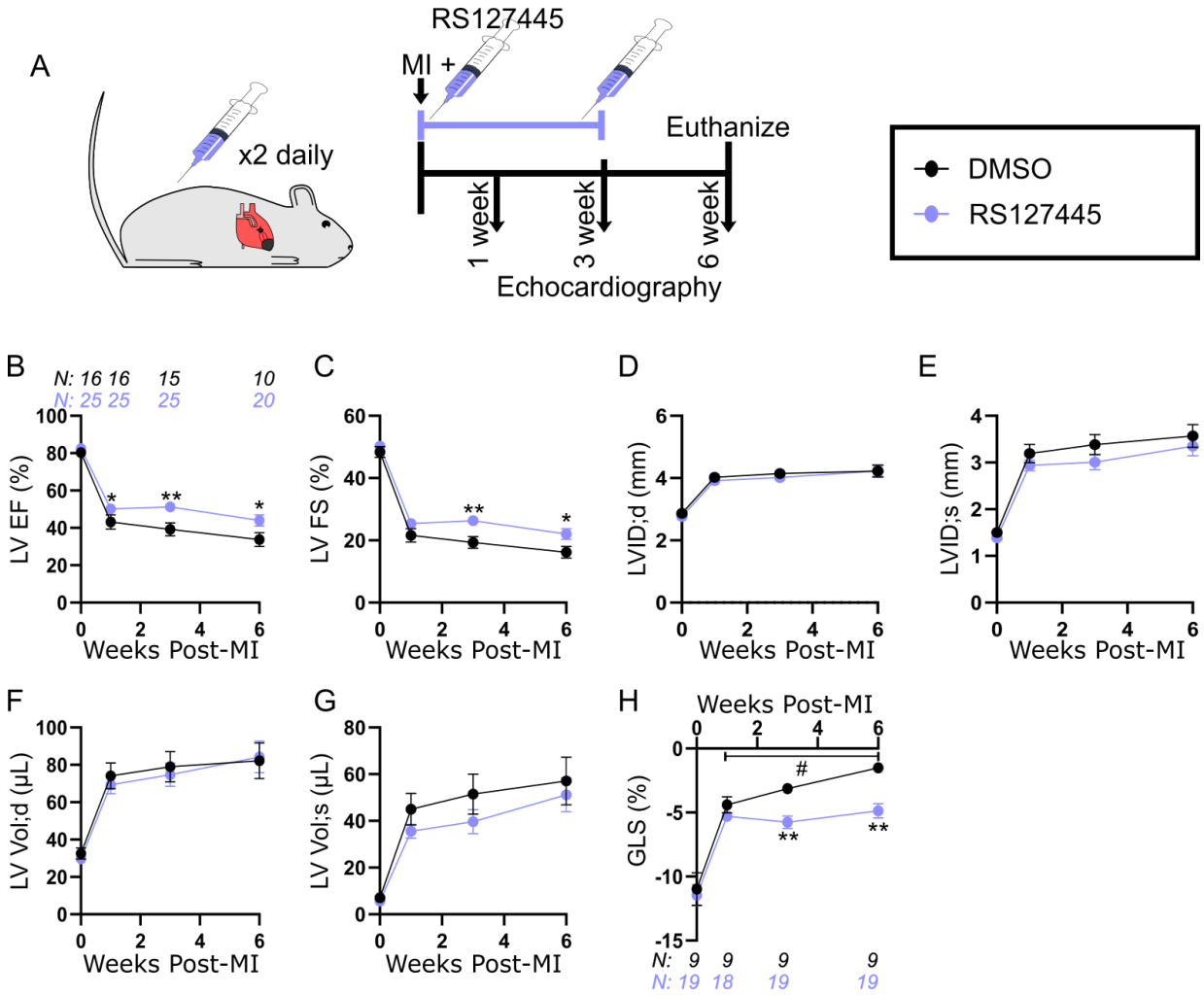

Supplemental Figure 4. Antagonism of 5-HT$_{2B}$ using the antagonist RS127445 (RS) improves outcomes after myocardial infarction (MI). A, Experimental approach. 12-week-old mice were subjected to MI surgery and coincidentally treated with dimethyl sulfoxide (DMSO) control or the 5-HT$_{2B}$ antagonist RS127445 with twice daily intraperitoneal injections. Treatment was ceased three weeks following injury and serial echocardiography was performed at times shown. **B,** Left ventricular ejection fraction (LV EF). **C,** Left ventricular fractional shortening (LV FS). **D,E,** Left ventricular internal dimension at end-diastole (LVID;d) and end-systole (LVID;s). **F,G,** Left ventricular volume at end-diastole (LV Vol;d) and end-systole (LV Vol;s). **H,** Global longitudinal strain (GLS). **B-H,** Mean ± SEM, *P<0.05, **P<0.01, between DMSO and RS treatments, #P<0.05 between previous timepoint within treatment group following 2-way ANOVA and Holm-Sidak post hoc test. Number of mice denoted in **B** applies to subsequent groups except **H** where explicitly labeled.

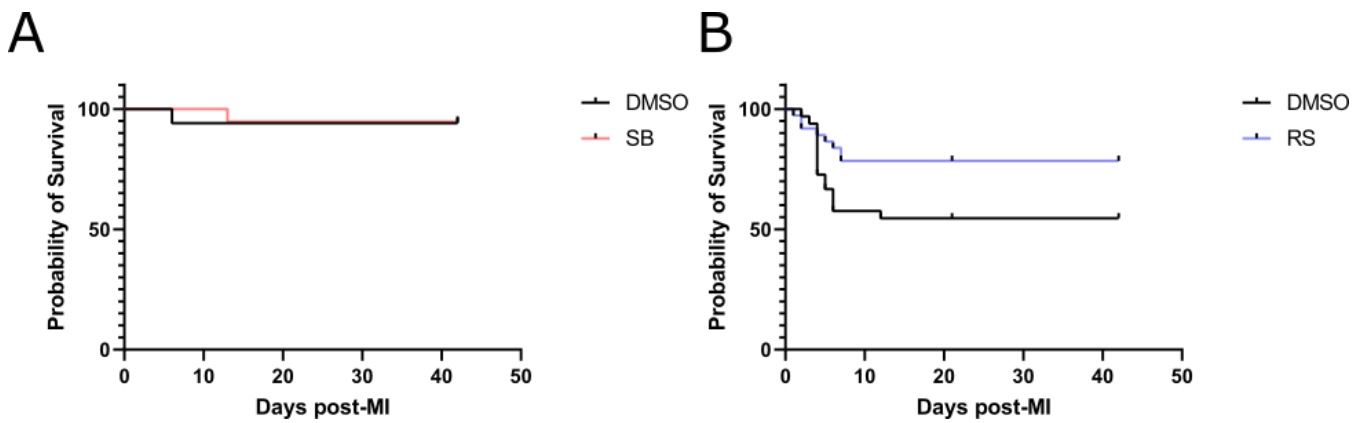

Supplemental Figure 5. Survival curve of 5-HT_{2B} antagonized mice following myocardial infarction (MI). A, No statistical difference in proportion of mice that survived post-MI. DMSO (N=16) and SB204741 (SB, N=19). **B,** No statistical difference in proportion of mice that survived post-MI. DMSO (N=33) and RS127445 (RS, N=37).

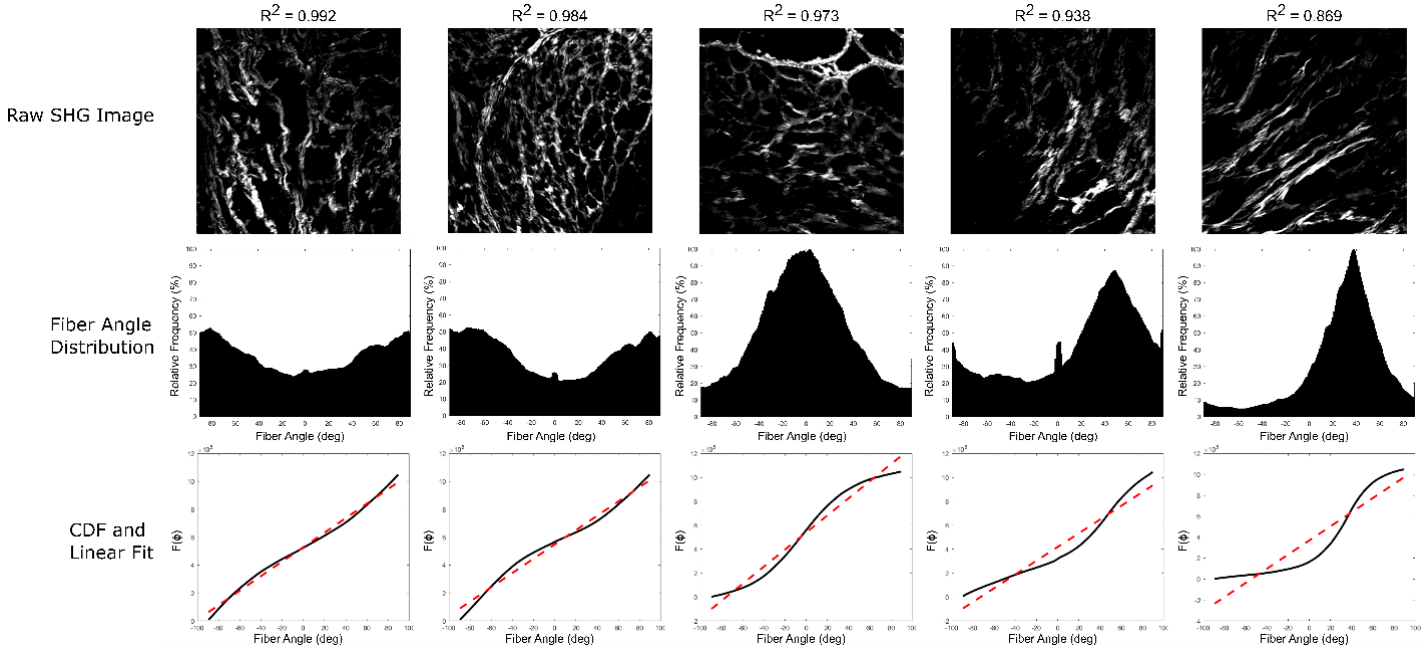

Supplemental Figure 6. Second harmonic generation (SHG) analysis and curve fitting to determine anisotropy. Top Row, Raw SHG images throughout the BZ organized from best (left) to worst (right) fit of a first-order polynomial. **Middle Row**, Distribution of fiber angles. As you move from left to right, peaks start to emerge which would result in anisotropic distribution. These peaks start to emerge at $R^2 < 0.98$ and the width of the peak thins and amplitude increase as R^2 decreases. **Bottom Row**, First-order polynomial fitting (red dashed line) to the cumulative distributive function (CDF) obtained from the distributions in the middle row.

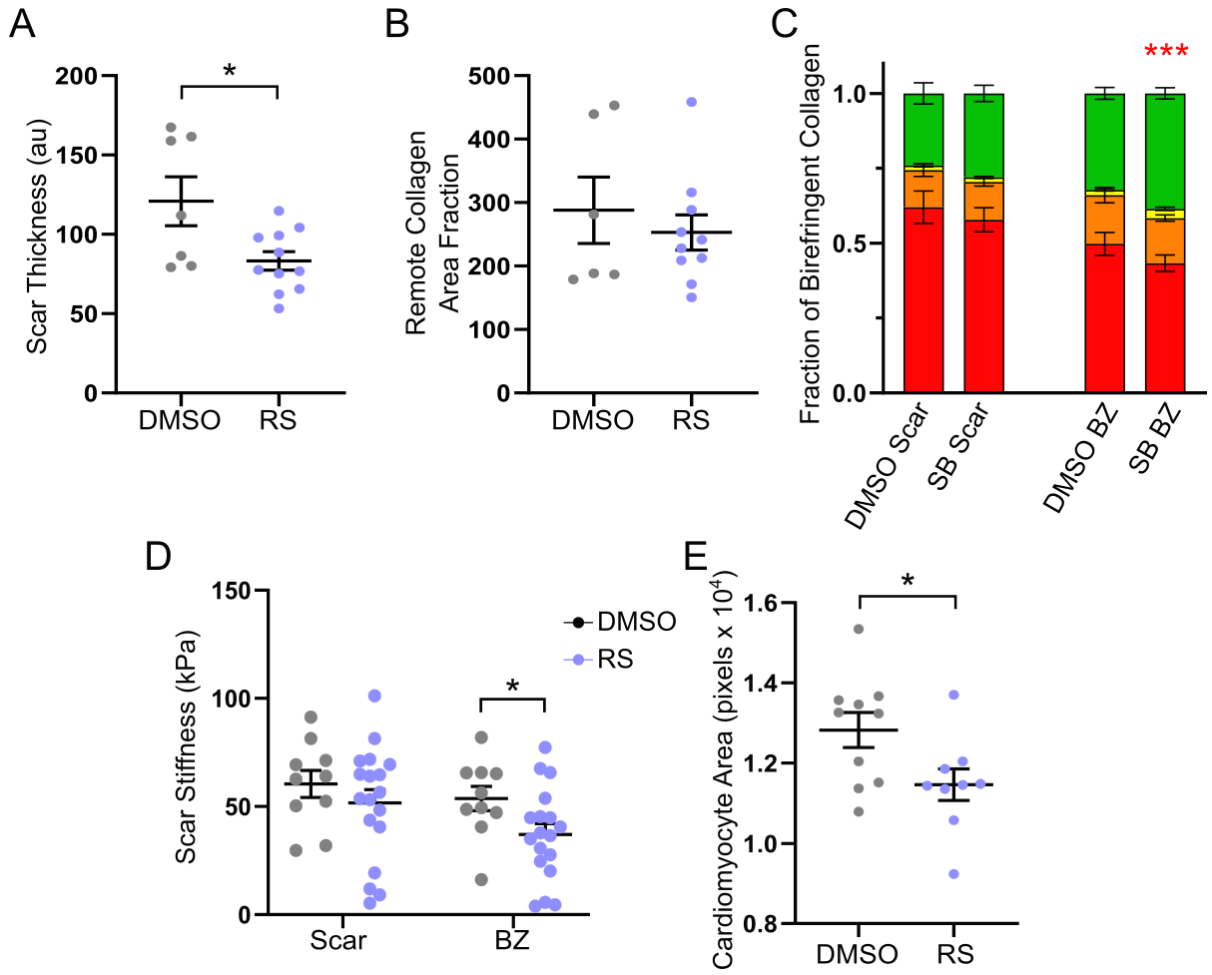

Supplemental Figure 7. Histological analysis of RS127445 (RS) treated mice demonstrates improved fibrotic remodeling compared to control animals. A, RS treatment decreases scar thickness six weeks after MI injury (N=7-11). **B,** No observed difference in interstitial fibrosis six weeks after MI (N=6-9) determined by picrosirius red (PSR) staining. **C,** PSR stain imaged under polarized light reveals a decrease in thick, mature collagen fibers in the border zone (BZ) of RS treated animals six weeks after MI (N=8-15). **D,** Tissue stiffness acquired by atomic force microscopy (AFM) reveals a marginal decrease in scar stiffness and a significant decrease in BZ stiffness with RS treatment six weeks after MI (N=10-18). **E,** Wheat germ agglutinin (WGA) staining of cardiomyocyte cell wall allows for the quantification of decreased short-axis cardiomyocyte cross-sectional area with RS treatment six weeks after MI (N=9-10). Mean ± SEM, *P<0.05, ***P<0.001, between dimethyl sulfoxide (DMSO) and RS treatments, following (**A, B, D,E**) 2-tailed Student *t* test or (**C**) 2-way ANOVA and Holm-Sidak post hoc test.

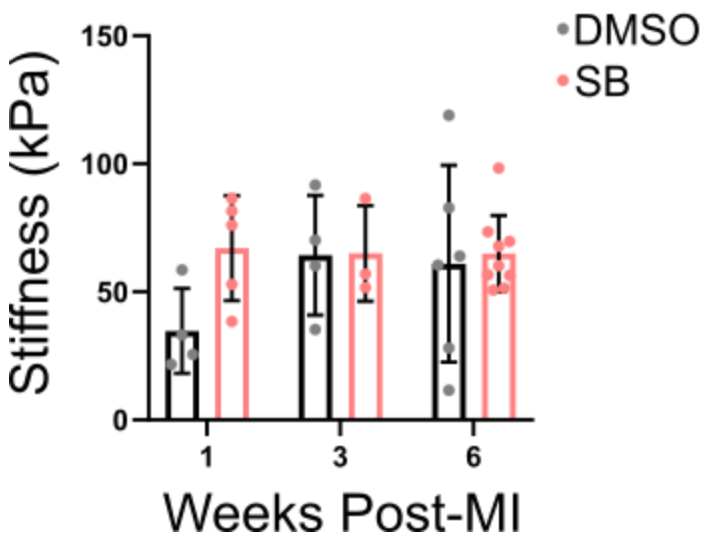

Supplemental Figure 8. Remote myocardial stiffness is not altered with SB204741 (SB) treatment. Atomic force microscopy (AFM) analysis was performed on cardiomyocytes in the left ventricle distant to the infarct zone. No changes in tissue stiffness were observed at any time point.

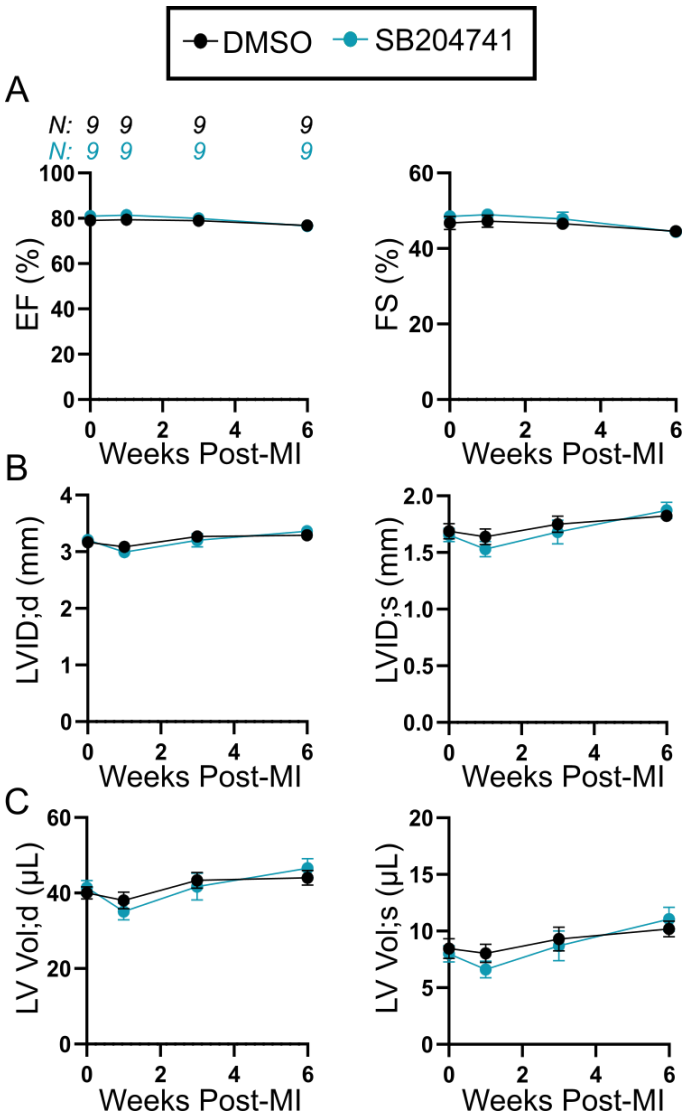

Supplemental Figure 9. 5-HT$_{2B}$ antagonism does not alter cardiac structure or function following sham operation. 12-week-old mice underwent sham operation. **A,** No difference in ejection fraction (EF) or fractional shortening (FS) was observed between dimethyl sulfoxide (DMSO) control and SB204741 (SB) treated mice. **B,** Left ventricular inner dimension (LVID) at both end-diastole and end-systole were similar between the two treatments. **C,** Left ventricular volume (LV Vol) at both end-diastole and end-systole were similar between the two treatments.

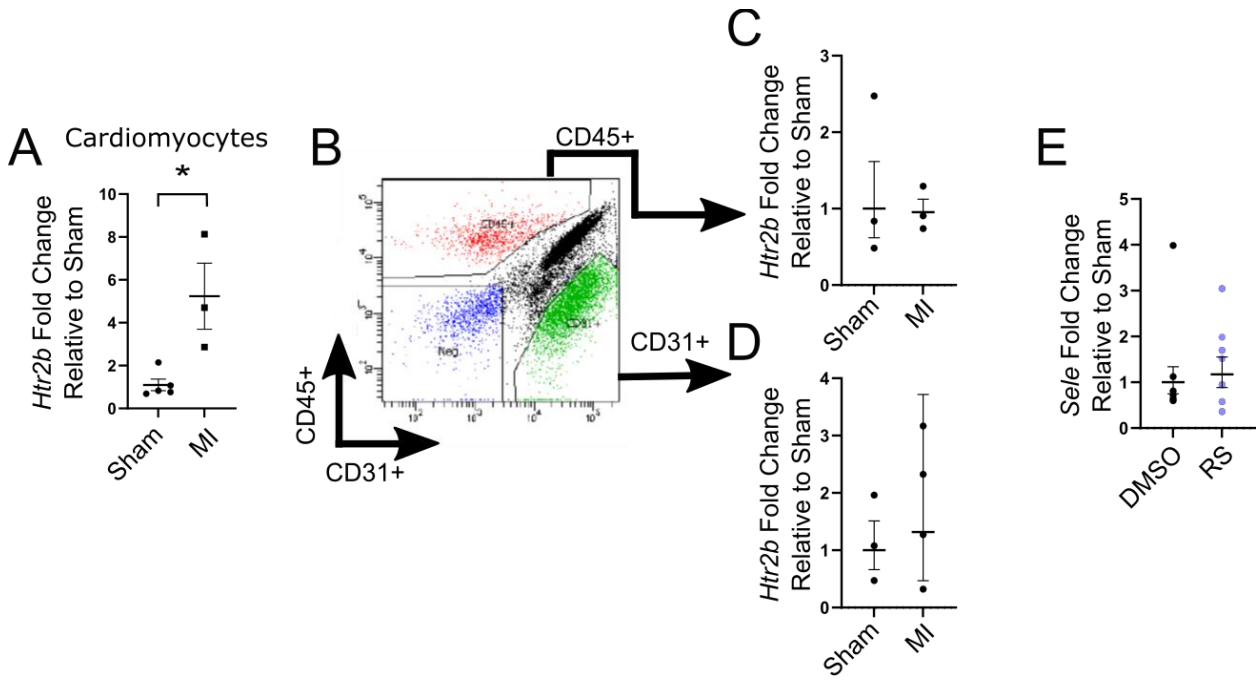

Supplemental Figure 10. *Htr2b* expression in isolated cell populations seven days after MI. **A,** *Htr2b* is increased in isolated cardiomyocytes after MI. **B,** FACS isolation of **C,** CD45+ and **D,** CD31+ cells reveals no increase in *Htr2b* expression after MI. **E,** *Sele* (gene encoding E-selectin) is not upregulated in scar tissue after MI indicating no change in endothelial cell activation. Mean ± SEM, *P<0.05, via 2-tailed Student *t* test**.**

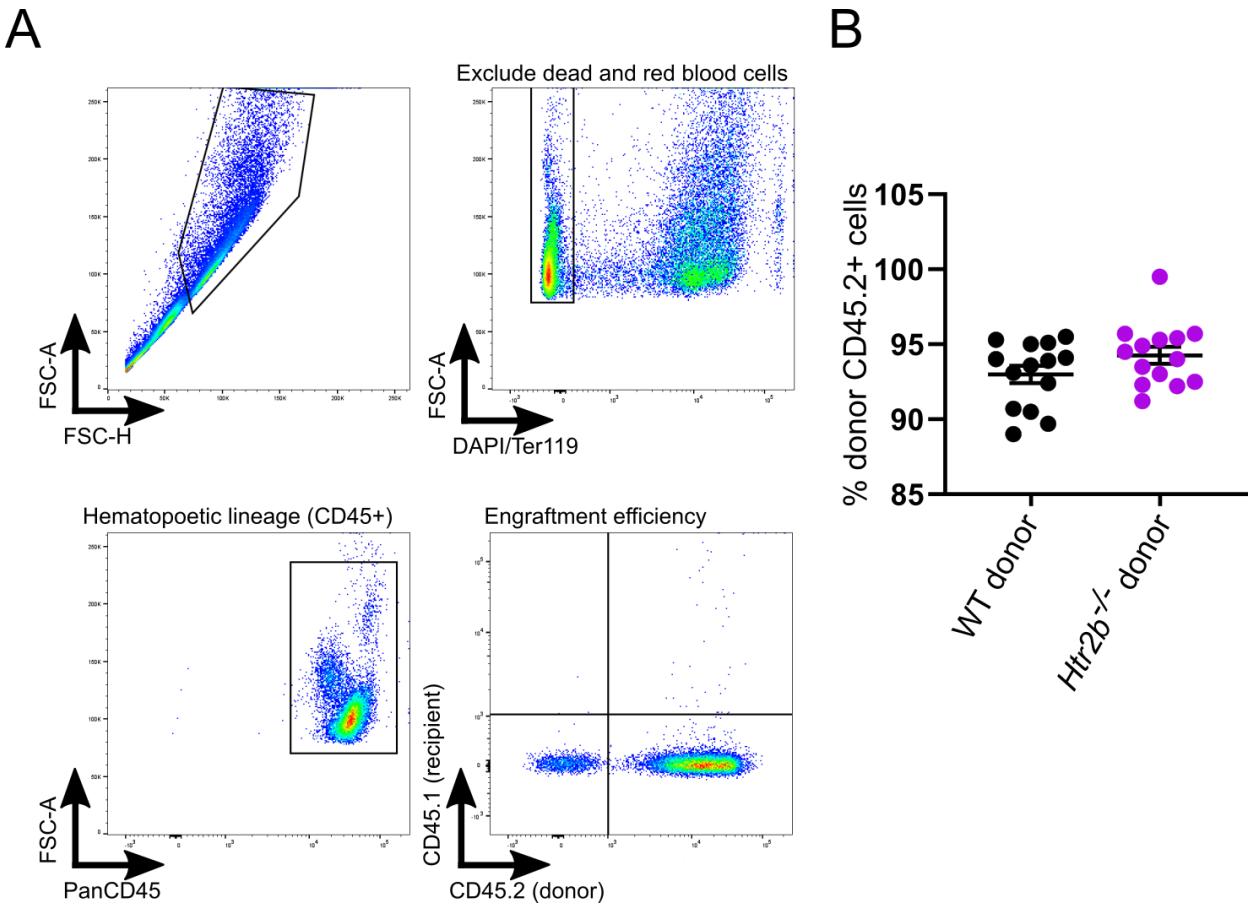

Supplemental Figure 11. Determination of bone marrow engraftment efficiency. **A,** Gating strategy to select for viable cells (excluding red blood cells), determine hematopoietic lineage (CD45+), and calculate engraftment efficiency (%CD45.2 donor cells of total CD45+ cells). **B,** Engraftment efficiencies for both wild-type (WT) recipients of both WT and *Htr2b*$^{-/-}$ donors.

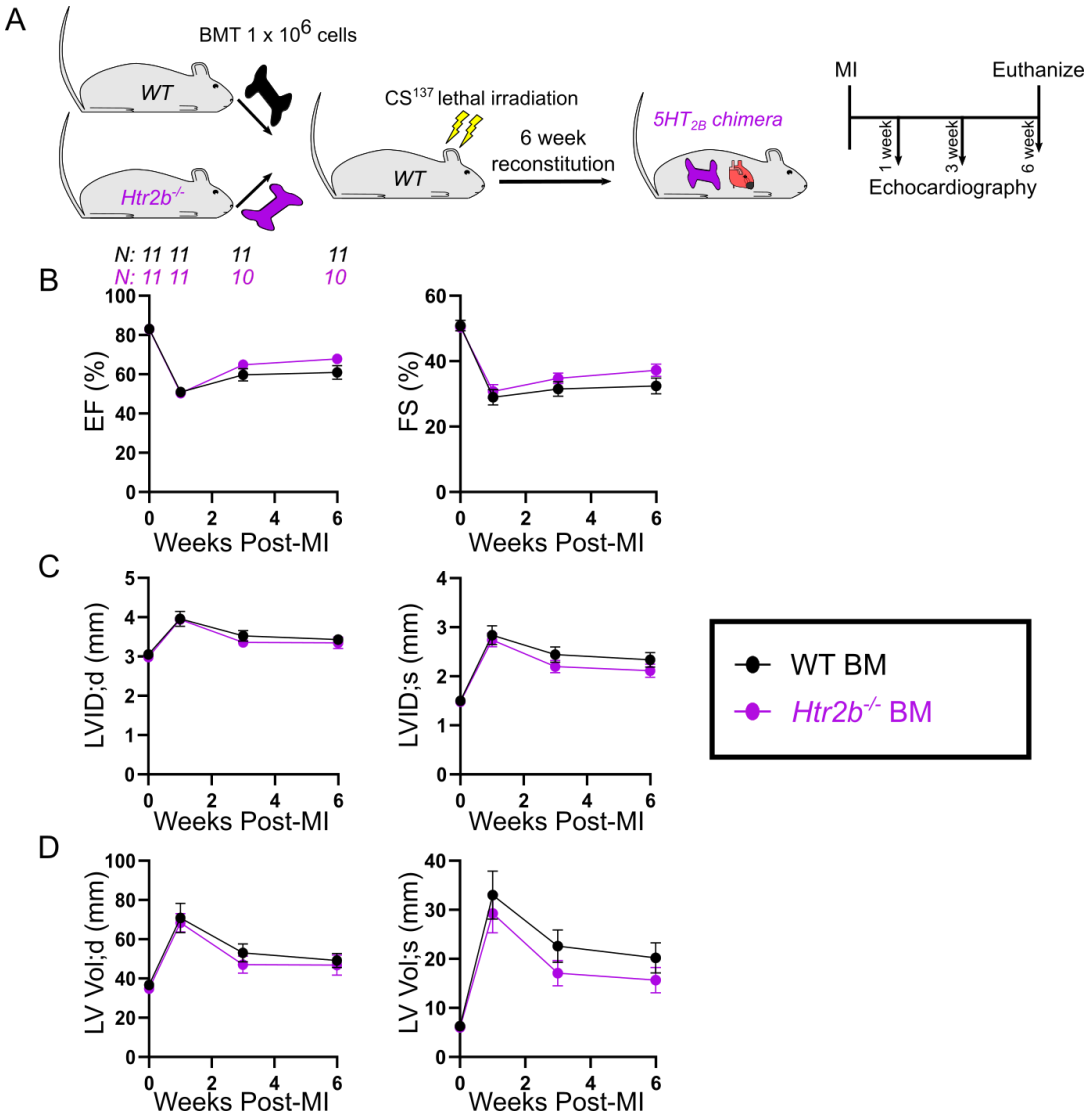

Supplemental Figure 12. Mice lacking 5-HT$_{2B}$ in bone marrow-derived cells do not exhibit an improved phenotype after myocardial infarction (MI) compared to mice with wild-type (WT) bone marrow. A, Experimental approach. Age- and sex-matched donors (WT or *Htr2b*$^{-/-}$) were transplanted into lethally irradiated WT mice and upon reconstitution, were subject to MI surgery and serial echocardiography. **B,** No difference in ejection fraction (EF) or fractional shortening (FS) was observed **C,** Left ventricular inner dimension (LVID) at both end-diastole and end-systole were similar between the two groups. **D,** Left ventricular volume (LV Vol) at both end-diastole and end-systole were similar regardless of bone marrow make-up.

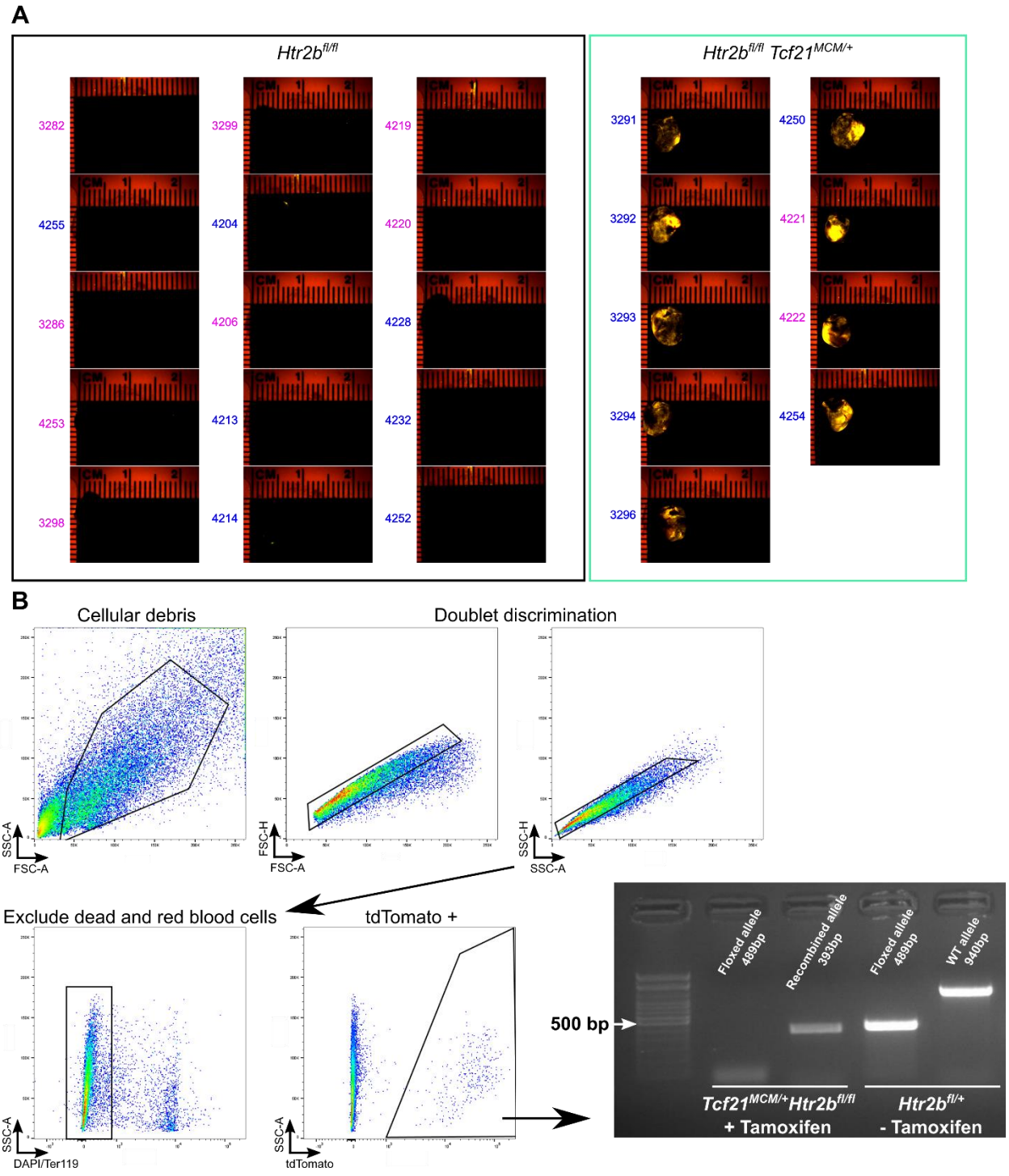

Supplemental Figure 13. Verification of Cre activation in *Htr2b$^{fl/fl}$Tcf21$^{MCM/+}$* animals. A, Control mice not harboring the MCM cDNA did not exhibit any fluorescent signal from the tdTomato reporter, whereas all mice harboring MCM cDNA under the control of the *Tcf21* promotor show fluorescent signal of the tdTomato reporter, indicating successful recombination. Mouse identifiers are color coded for male (blue) and female (pink). All images (control and experimental groups) acquired under the same imaging parameters with the same

brightness/contrast adjustments made in ImageJ. **B,** PCR validating recombination efficiency. tdTomato+ cells were isolated and PCR was run to identify the recombined allele (second lane) compared with a control reaction which would amplify the non-recombined floxed allele (first lane) if present.

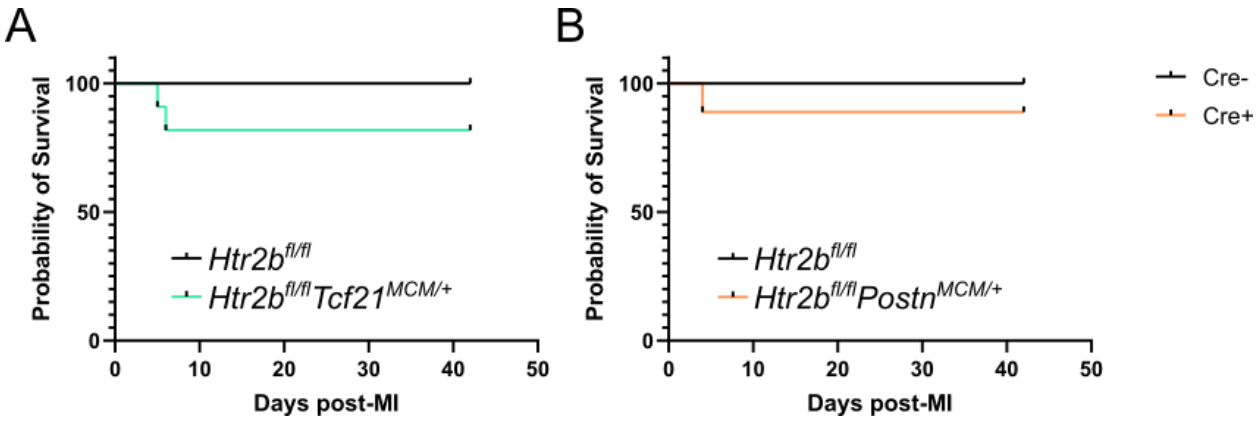

Supplemental Figure 14. Survival of resident fibroblast and myofibroblast knockout animals. A, There was no statistical difference in the survival of *Htr2b*$^{fl/fl}$ control animals (N=15) compared to *Htr2b*$^{fl/fl}$*Tcf21*$^{MCM/+}$ animals (N=11). **B,** There was no statistical difference in the survival of *Htr2b*$^{fl/fl}$ control animals (N=4) compared to *Htr2b*$^{fl/fl}$*Postn*$^{MCM/+}$ animals (N=9).

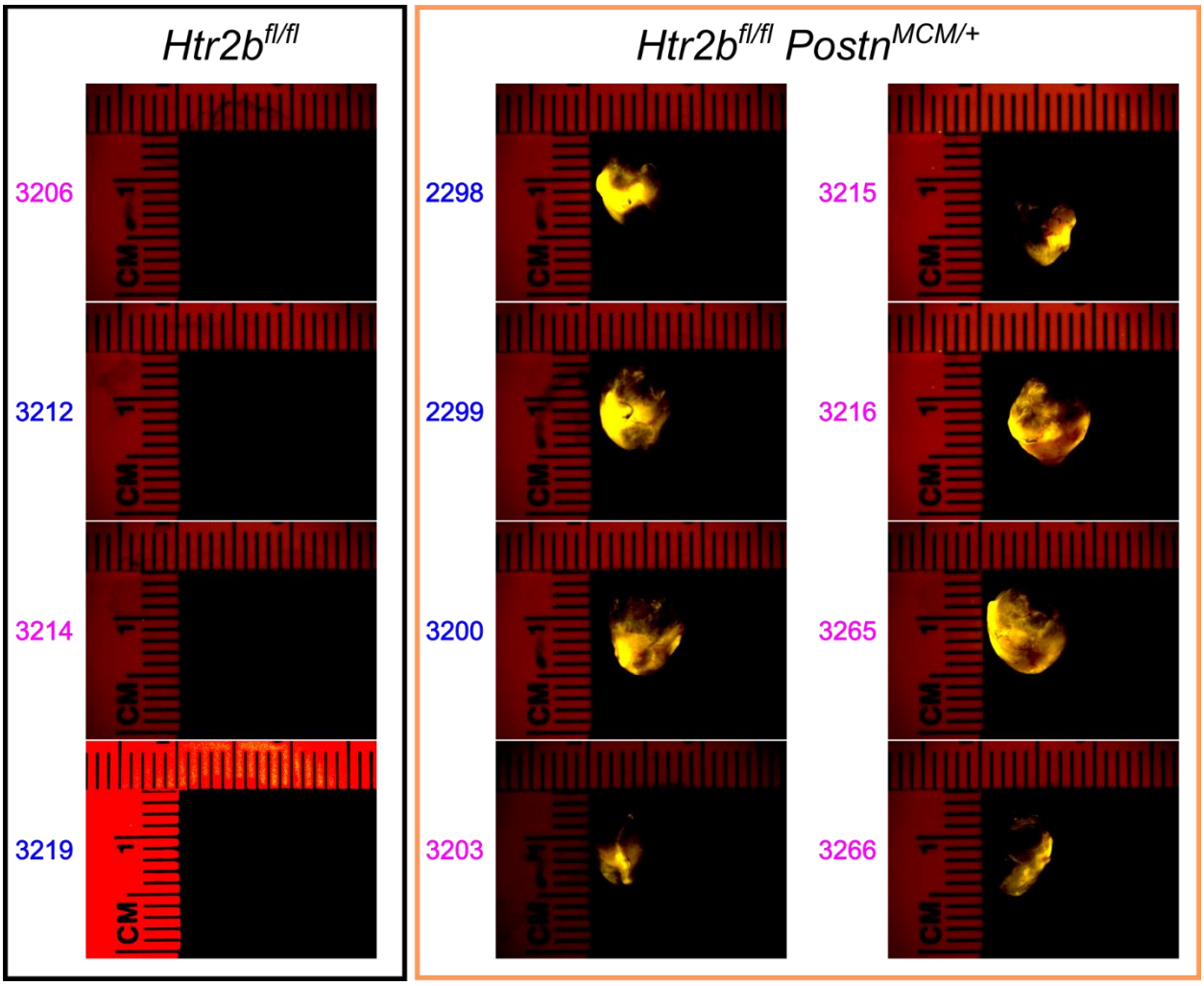

Supplemental Figure 15. Verification of Cre activation in *Htr2b*$^{fl/fl}$*Postn*$^{MCM/+}$ animals. Control mice not harboring the MCM cDNA did not exhibit any fluorescent signal from the tdTomato reporter, whereas all mice harboring MCM cDNA under the control of the *Postn* promotor show fluorescent signal of the tdTomato reporter, indicating successful recombination. Mouse identifiers are color coded for male (blue) and female (pink). All images (control and experimental groups, except 3219 overexposed for emphasis) acquired under the same imaging parameters with the same brightness/contrast adjustments made in ImageJ.

A

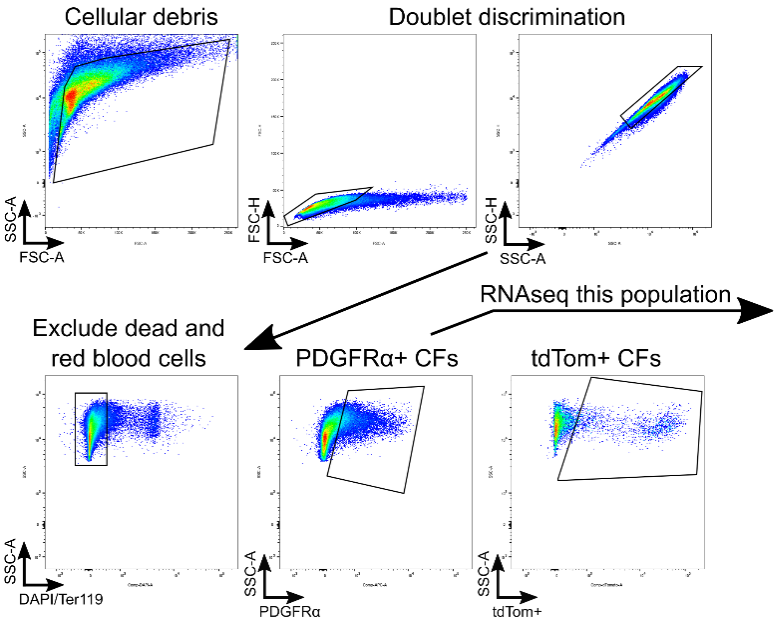

B

Mouse ID	RIN	Total Reads	Mapped Reads	Percent Aligned	Percent tdTom+
Htr2b$^{fl/fl}$					
6	9.3	70826758	69942731	98.75	0.00
5	9.2	93422980	91778498	98.24	0.00
Htr2b$^{fl/fl}$*Postn*$^{MCM/+}$					
7	9.6	90420754	87771218	97.07	14.20
4	8.6	89413414	83571864	93.47	23.50
1	6.6	78616202	73991839	94.12	14.40
2	5.9	85407778	83312403	97.55	24.30
Summary					
Average	8.2	84684648	81728092	96.53	19.10
SEM	0.6	3468970	3377296	0.90	2.78

Supplemental Figure 16. PDGFRα+ cell isolation and RNA-sequencing quality control. A, PDGFRα+ cells were isolated from injured tissue of *Htr2b*$^{fl/fl}$ and *Htr2b*$^{fl/fl}$*Postn*$^{MCM/+}$ mice seven days after MI for sequencing. **B,** Table detailing quality of RNA integrity (RIN), quality of alignment, and the percentage of cells with a recombined *Htr2b* allele which underwent RNA sequencing.

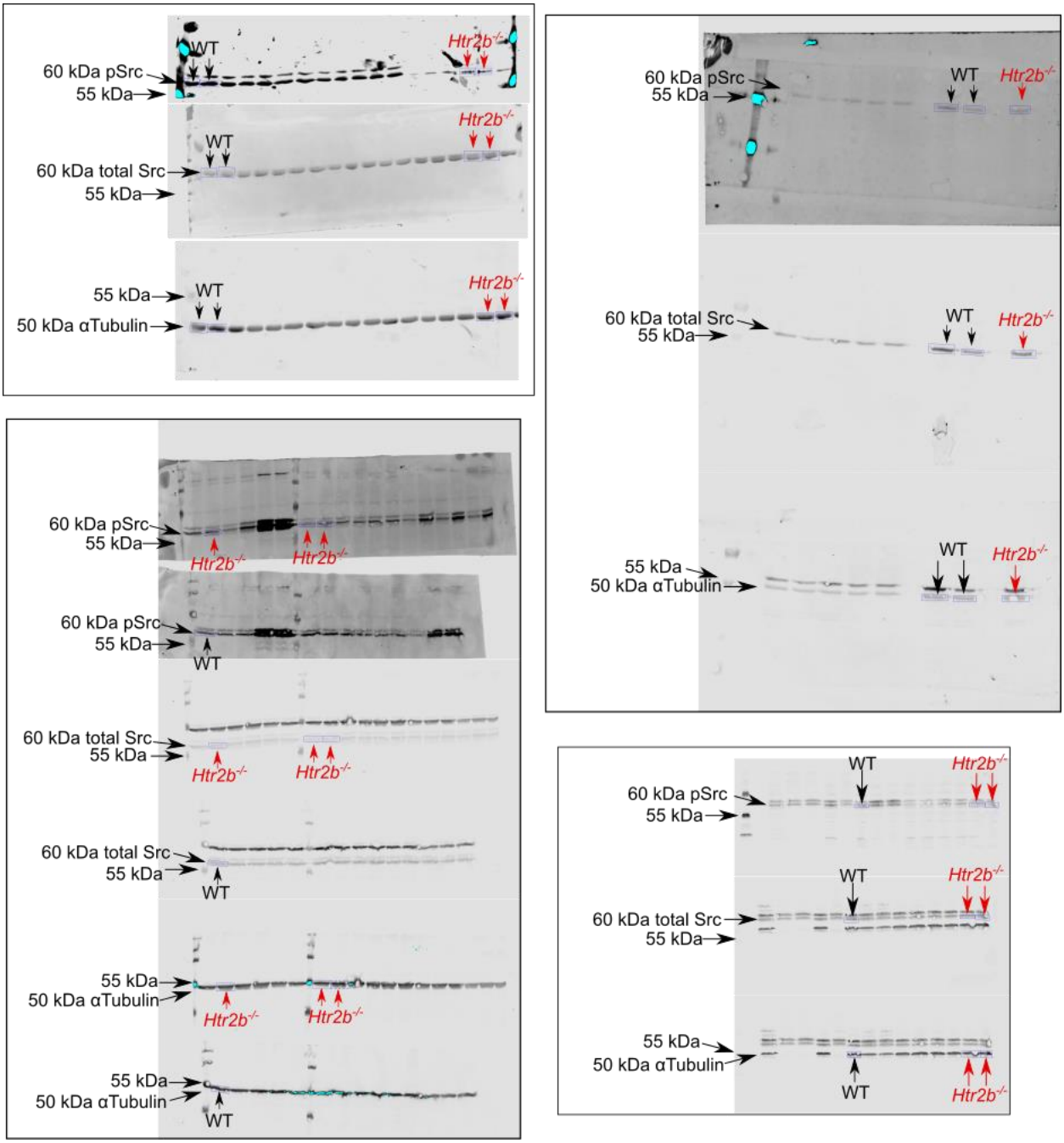

Supplemental Figure 17. Raw western blot images for pSrc quantification. Four independent experiments with black arrows indicating wild-type (WT) and red arrows indicating *Htr2b*$^{-/-}$ cardiac fibroblasts.

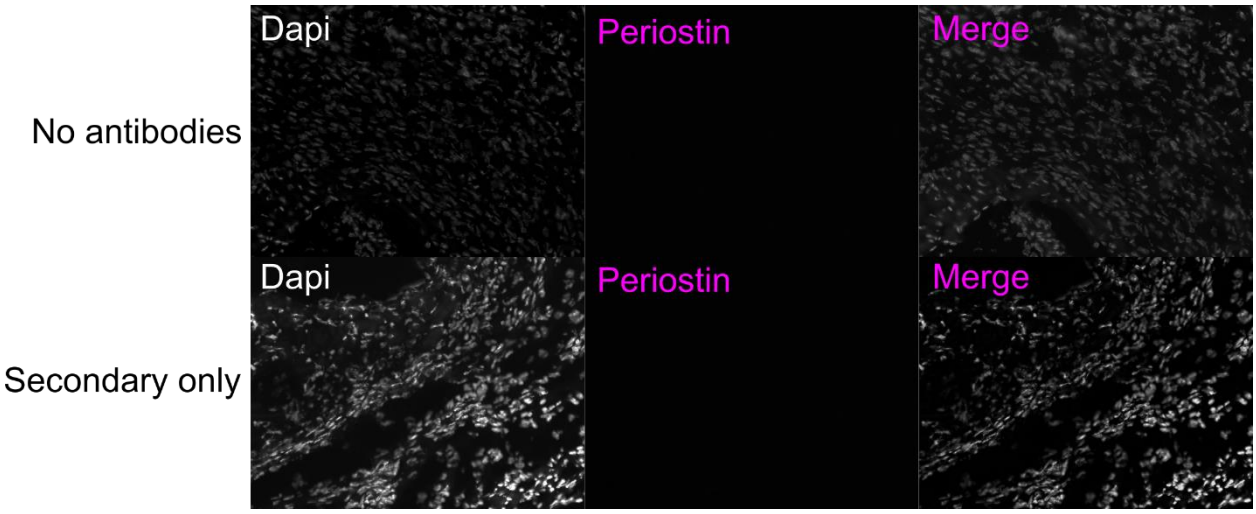

Supplemental Figure 18. Controls for periostin immunostaining. Unstained control (top) and secondary only control (bottom) imaged under identical settings as experimental samples.

Supplemental Table 1. Heart rate ± SEM.

Experiment	Day 0	Day 42
DMSO vs. SB204741		
DMSO	652.7 ± 9.5	689.4 ± 2.5
SB204741	671.0 ± 6.3	676.8 ± 5.1
DMSO vs. RS127445		
DMSO	653.7 ± 13.5	696.6 ± 13.5
RS127445	658.2 ± 13.9	699.9 ± 14.1
Htrb2b$^{fl/fl}$ **vs.** ***Htr2b$^{fl/fl}$Tcf21$^{MCM/+}$***		
Htrb2b$^{fl/fl}$	592 ±13.6	621.1 ± 17.1
Htr2b$^{fl/fl}$Tcf21$^{MCM/+}$	590 ±21.1	662.1 ± 6.2
Htrb2b$^{fl/fl}$ **vs.** ***Htr2b$^{fl/fl}$Postn$^{MCM/+}$***		
Htrb2b$^{fl/fl}$	584.1 ± 22.2	663.2 ± 26.2
Htr2b$^{fl/fl}$Postn$^{MCM/+}$	575.6 ± 16.0	638.4 ± 5.5

Supplemental Table 2. Significantly altered GO terms from RNA sequencing (BP = biological process, CC = cellular component).

ID	ONTOLOGY	Description
GO:0098813	BP	nuclear chromosome segregation
GO:0000819	BP	sister chromatid segregation
GO:0033047	BP	regulation of mitotic sister chromatid segregation
GO:0033045	BP	regulation of sister chromatid segregation
GO:0007059	BP	chromosome segregation
GO:0000070	BP	mitotic sister chromatid segregation
GO:0051983	BP	regulation of chromosome segregation
GO:0000793	CC	condensed chromosome
GO:0000779	CC	condensed chromosome, centromeric region
GO:0000775	CC	chromosome, centromeric region
GO:0000780	CC	condensed nuclear chromosome, centromeric region
GO:0098687	CC	chromosomal region
GO:0000777	CC	condensed chromosome kinetochore
GO:0000940	CC	condensed chromosome outer kinetochore
GO:0000778	CC	condensed nuclear chromosome kinetochore
GO:0000776	CC	kinetochore

Supplemental Table 3. Primer sets used for qPCR.

Target	Forward Primer (5' to 3')	Reverse Primer (5' to 3')
Gapdh	ATGACAATGAATACGGCTACAG	TCTCTTGCTCAGTGTCCTTG
Hprt1	CCCCAAAATGGTTAAGGTTGC	AACAAAGTCTGGCCTGTATCC
Nppb	GCACAAGATAGACCGGATCG	CCCAGGCAGAGTCAGAAAC
Dnajb4	ATATAGTGGCTGCACCAAACG	CCTTCCCTCGGAAAAGTGATTT
Htr2b	TCAATAGGCATCGCCATCCCAG	CCATGATGGTGAGAGGTGCGAA
Htr2a	AACCCCATTCACCATAGCC	TGCCACAAAAGAGCCTATGAG
Sele	ATGCCTCGCGCTTTCTCTC	GTAGTCCCGCTGACAGTATGC